BIOCHEMISTRY
including biophysical chemistry & molecular biology

Article

pubs.acs.org/biochemistry

Assembly of the SLIP1−SLBP Complex on Histone mRNA Requires Heterodimerization and Sequential Binding of SLBP Followed by SLIP1

Nitin Bansal,[†] Minyou Zhang,[†,‡] Aishwarya Bhaskar,[†] Patrick Itotia,[†] EunHee Lee,[§] Lyudmila S. Shlyakhtenko,[∥] TuKiet T. Lam,[⊥] Andrew Fritz,[@] Ronald Berezney,[@] Yuri L. Lyubchenko,[∥] Walter F. Stafford,[§] and Roopa Thapar*[,†,‡,#]

[†]Hauptman-Woodward Medical Research Institute, 700 Ellicott Street, Buffalo, New York 14203, United States

[‡]Department of Structural Biology, SUNY at Buffalo, 700 Ellicott Street, Buffalo, New York 14203, United States

[§]Boston Biomedical Research Institute, 64 Grove Street, Watertown, Massachusetts 02472-2829, United States

[∥]Department of Pharmaceutical Sciences, College of Pharmacy, University of Nebraska Medical Center, Omaha, Nebraska 68198-6025, United States

[⊥]W. M. Keck Foundation Biotechnology Resource Laboratory, Yale University, New Haven, Connecticut 06511, United States

[@]Department of Biological Sciences, SUNY at Buffalo, Buffalo, New York 14260, United States

Supporting Information

ABSTRACT: The SLIP1−SLBP complex activates translation of replication-dependent histone mRNAs. In this report, we describe how the activity of the SLIP1−SLBP complex is modulated by phosphorylation and oligomerization. Biophysical characterization of the free proteins shows that whereas SLIP1 is a homodimer that does not bind RNA, human SLBP is an intrinsically disordered protein that is phosphorylated at 23 Ser/Thr sites when expressed in a eukaryotic expression system such as baculovirus. The bacterially expressed unphosphorylated SLIP1−SLBP complex forms a 2:2 high-affinity (K_D < 0.9 nM) heterotetramer that is also incapable of binding histone mRNA. In contrast, phosphorylated SLBP from baculovirus has a weak affinity (K_D ~3 μM) for SLIP1. Sequential binding of phosphorylated SLBP to the histone mRNA stem−loop motif followed by association with SLIP1 is required to form an "active" ternary complex. Phosphorylation of SLBP at Thr171 promotes dissociation of the heterotetramer to the SLIP1−SLBP heterodimer. Using alanine scanning mutagenesis, we demonstrate that the binding site on SLIP1 for SLBP lies close to the dimer interface. A single-point mutant near the SLIP1 homodimer interface abolished interaction with SLBP in vitro and reduced the abundance of histone mRNA in vivo. On the basis of these biophysical studies, we propose that oligomerization and SLBP phosphorylation may regulate the SLBP−SLIP1 complex in vivo. SLIP1 may act to sequester SLBP in vivo, protecting it from proteolytic degradation as an inactive heterotetramer, or alternatively, formation of the SLIP1−SLBP heterotetramer may facilitate removal of SLBP from the histone mRNA prior to histone mRNA degradation.

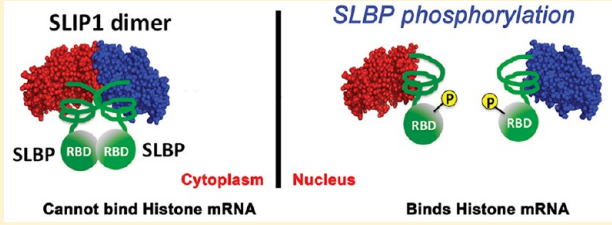

Replication-dependent histone mRNAs synthesize histone proteins that package newly replicated DNA into chromatin.[1] Instead of a poly(A) tail, they end in a 26-nucleotide stem−loop structure in their 3′UTR. This sequence forms the binding site for stem−loop binding protein (SLBP).[2] SLBP functions in processing of the histone pre-mRNA in the nucleus,[3] in export of the histone mRNP[4] to the cytoplasm, and in translation[5] and regulation of the stability[6] of the histone mRNA. Similar to the poly(A) tail on poly(A)-containing mRNAs, the stem−loop cis element at the 3′ end of histone mRNAs is necessary for efficient histone protein synthesis in vivo[6−8] (Figure 1A of the Supporting Information). Early studies showed that the histone mRNA stem−loop was necessary for enhancing the translational efficiency as well as the stability of the mRNA,[9] and like the poly(A) tail, it synergizes with the cap to stimulate translation in vivo.[9] SLBP is also required for the translation of histone mRNAs and is found on polysomes in the presence of an intact stem−loop.[5,10,11] In a heterologous yeast system using reporter mRNAs, the physical interaction of SLBP with the translation initiation machinery was found to require eIF4G and eIF3[10] (Figure 1A of the Supporting Information). The translation regulatory functions of SLBP have been mapped using deletion mutagenesis to a 15-amino acid region in the N-terminal domain of human SLBP[5] (Figure 1C of the Supporting Information). Multiple interactions between SLBP and the

Received: August 9, 2012
Revised: December 19, 2012
Published: January 3, 2013

eIF4F complex have been proposed,[10−12] yet the molecular details of these complexes and the mechanism of SLBP-mediated translation regulation remain to be understood.

Recently, another histone mRNA-specific translation initiation factor was identified in mammalian cells called SLBP-interacting protein (SLIP1)[12] (Figure 1B of the Supporting Information). Human SLIP1 (hSLIP1) is important for upregulating histone protein synthesis via a direct protein−protein interaction with SLBP. hSLIP1 is a 222-amino acid protein ($M_r \sim 26$ kDa) that on the basis of sequence homology, belongs to the "middle domain of eukaryotic initiation factor 4G domain" (MIF4GD) family of proteins in the Pfam database[13−15] (Figure 1B of the Supporting Information). Other members of the MIF4GD family that are homologous to hSLIP1 include the middle domain of eIF4G,[16] PAIP1,[17] DAP5,[18] PDCD4,[19] Upf2,[20] CTIF,[21] and CBP80.[22] hSLIP1 interacts specifically with the 15-residue translation activation region in *Xenopus* SLBP1 (also conserved in human SLBP) and stimulates the translation of histone mRNAs in *Xenopus* oocytes.[12]

It is not known how hSLIP1 and hSLBP regulate the translation of histone mRNAs. The proposed model is one in which hSLIP1 may form a bridge between hSLBP and the eIF4F initiation complex at the 5′ end of the mRNA[12] (Figure 1A of the Supporting Information). Direct association of hSLIP1 with eIF3 has recently been shown to be important for efficient histone mRNA translation.[23] The crystal structure of a protein (UniProt entry Q5EAQ1) from *Danio rerio* (zebrafish) that is 72% identical in sequence to hSLIP1 (Figure 2 of the Supporting Information) has been determined to a resolution of 1.92 Å as a protein of unknown function as part of the CESG Structural Genomics Consortium [Protein Data Bank (PDB) entry 2I2O][24] (Figure 1B of the Supporting Information). The protein has been annotated as MIF4Gdb in the UniProt knowledgebase. MIF4Gdb is a homodimer in the asymmetric unit in the crystal (Figure 1B of the Supporting Information), although several dimers pack against each other in the unit cell. Each MIF4Gdb homodimer is a crescent-shaped molecule composed of 13 α-helices and two 3_{10}-helices that forms six HEAT-like motifs.[25] Each monomer resembles the middle domain of eIF4G (MIF4G) in its overall folding topology. The overall structure[23] is consistent with MIF4Gdb being a molecular adaptor that could act as a scaffold for protein−protein interactions to help assemble components of the protein translation machinery.

To understand the structure and mechanism of assembly of hSLBP and hSLIP1 proteins on histone mRNA, we formed complexes of unphosphorylated and phosphorylated full-length human SLBP (hSLBP) with hSLIP1 and characterized their biophysical properties by gel filtration, analytical ultracentrifugation (AUC), and atomic force microscopy (AFM). We report that the unphosphorylated hSLBP−hSLIP1 complex exists in a 2:2 stoichiometry to form a high-affinity (K_D < 0.9 nM) heterotetramer that is incapable of binding histone mRNA. Formation of the hSLBP−hSLIP1−histone mRNA ternary complex requires pre-binding of the hSLBP monomer to the histone mRNA stem−loop, followed by interaction with hSLIP1. Characterization of the bacterially expressed translation activation domain of hSLBP (residues 1−110) by NMR spectroscopy shows that the N-terminal domain of hSLBP is disordered in solution. Using mass spectrometry, we have identified 23 new phosphorylation sites in the baculovirus-expressed hSLBP protein that may also be sites of phosphorylation in mammalian cells. To identify the binding interface on hSLIP1 for hSLBP, we used the structure of MIF4Gdb as a guide to design a number of single-site mutants in hSLIP1. The affinity of mutant hSLIP1 proteins for full-length baculovirus-expressed hSLBP was measured by Surface Plasmon Resonance (SPR). A single-point mutant R202A hSLIP1 that lies close to the hSLIP1 homodimer interface abrogated binding to hSLBP in vitro but had no effect on the structure or oligomeric properties of hSLIP1. In vivo biological studies confirmed the importance of this residue in regulating histone mRNA abundance. These data support a model in which both oligomerization and phosphorylation play important regulatory roles in the assembly of the hSLBP−hSLIP1−RNA complex. The functional implications of hSLBP−hSLIP1 complex hetero-oligomerization and hSLBP phosphorylation for regulation of histone gene expression are discussed.

EXPERIMENTAL PROCEDURES

Protein Expression. Full-length phosphorylated human SLBP was expressed in a baculovirus expression system as previously described.[26] hSLIP1, hSLIP1 mutants, and the N-terminal domain of hSLBP (residues 1−110, WT and W75A) were expressed as $(His)_6$-tagged proteins from vector pET28a (Novagen). The proteins were purified using Ni^{2+} affinity and gel filtration chromatography using standard protocols. hSLIP1 and hSLBP mutants were made using Quickchange mutagenesis (Stratagene). Uniformly ^{15}N-labeled and ^{15}N- and ^{13}C-labeled N-terminal domains (hSLBP-ND) of WT and W75A hSLBP (1−110) were generated for NMR studies by expressing the proteins in M9 minimal medium with [^{15}N]ammonium chloride and [^{13}C]glucose as the sole sources of ^{15}N and ^{13}C, respectively. MIF4Gdb from *D. rerio* was expressed as a maltose-binding protein (MBP) fusion protein. The MBP tag was cleaved with TEV protease. hSLIP1 was co-expressed with full-length hSLBP in *Escherichia coli* from vector pRSF-Duet (Novagen). The hSLIP1 protein has a $(His)_6$ tag, whereas hSLBP was untagged. The complex was purified using nickel affinity chromatography followed by gel filtration chromatography. The mutant (R202A hSLIP1−hSLBP) and the N-terminal domain of human SLBP (residues 1−100) (hSLIP1−hSLBP100) complexes were expressed and purified like the wild-type hSLIP1−hSLBP complex. Formation of the complex between the respective proteins was monitored on a HiPrep Sephacryl 200 26/60 column (GE) equilibrated in phosphate-buffered saline (pH 7.4) and run at a flow rate of 0.5 mL/min. The column was standardized with RNase A, carbonic anhydrase, cytochrome *c*, BSA, and blue dextran.

Mass Spectrometry. Baculovirus-expressed phosphorylated hSLBP proteins were treated with a chloroform/water/methanol mixture to remove trace amounts of detergent. The intact protein mass was determined on a Waters Qtof-Micro mass spectrometer, with detailed sample preparation and instrument parameter settings described in the Supporting Information.

For the determination of phosphorylation sites of hSLBP, full-length hSLBP was enzymatically digested, phosphopeptides were enriched with titanium oxide, and liquid chromatography with tandem mass spectrometry (LC−MS/MS) was performed on an LTQ Orbitrap Elite MS system. Data were searched utilizing a MASCOT Protein Search engine. Detailed methods for sample preparation, instrument settings, and database searching are described in the Supporting Information.

NMR Spectroscopy. hSLBP and hSLIP1 proteins used for NMR experiments were dissolved in 20 mM Tris-acetate buffer, 50 mM NaCl, and a 90% H_2O/10% D_2O mixture (pH 6.0). NMR data were collected on either a Varian Inova 600 MHz spectrometer equipped with a 5 mM z-gradient triple-resonance probe or an Inova 700 MHz spectrometer with a cryoprobe. Heteronuclear NMR experiments used to obtain backbone assignments of human SLBP (residues 1−110, W75A) were two-dimensional (2D) $^{1}H-^{15}N$ HSQC, $^{1}H-^{13}C$ HSQC, three-dimensional (3D) HNCA, 3D HN(CO)CA, 3D CBCA(CO)-NH, 3D HNCACB, and 3D CCC-TOCSY. A 75 ms 3D $^{15}N-^{1}H$ NOESY-HSQC spectrum was also collected. Information about backbone dynamics was obtained from measurement of ^{15}N relaxation rates. ^{15}N T_1 and T_2 relaxation rates and steady-state $\{^{1}H\}-^{15}N$ NOEs were measured using well-established pulse sequences.[27] All relaxation rate and steady-state $\{^{1}H\}-^{15}N$ NOE experiments were conducted at 25 °C and 600 MHz. For the T_1 experiments, 512 × 256 complex points were collected with relaxation delay times of 10, 100, 200, 300, 400, 600, 800, 1000, and 1200 ms; the T_2 experiments were performed with relaxation delay times of 14.4, 28.8, 57.6, 86.4, 100.8, 115.2, 129.6, 144, 158.4, and 172.8 ms. The steady-state $\{^{1}H\}-^{15}N$ NOE experiment was performed by collecting two identical data sets recorded with and without proton presaturation. The saturation period consisting of a train of 120° proton pulses was 4.9 s. The interscan delay period was 5 s. NMR chemical shift mapping experiments were performed on an Inova 700 MHz spectrometer equipped with a cryoprobe. Unlabeled hSLIP1 was titrated into a solution of ^{15}N-labeled hSLBP-ND, and the perturbations were mapped in the hSLBP-ND $^{1}H-^{15}N$ TROSY spectrum as a function of increasing SLIP1 concentration.

Analytical Ultracentrifugation (AUC). Sedimentation velocity experiments were performed on a Beckman Optima XL-I analytical ultracentrifuge equipped with Rayleigh optics. The cells were equipped with sapphire windows and 12 mm charcoal-filled Epon centerpieces. Apparent sedimentation coefficient distribution patterns were computed by the time derivative method.[28−30] The hSLIP1 dimer and hSLBP−hSLIP1 complex fractions from gel filtration were dialyzed extensively against phosphate-buffered saline (PBS) at 4 °C overnight and then subjected to AUC at 50000 rpm and 20 °C. The molar mass was computed from sedimentation velocity profiles using SEDANAL, which uses a nonlinear least-squares curve fitting algorithm to fit data to solutions of the differential equation (the Lamm equation) describing sedimentation. Fits were performed on time difference data to remove the time-independent systematic baseline components. Values of s and D produced by the fitting procedure were substituted into the Svedberg equation to obtain the molar mass of the protein, M_2:

$$M_2 = \frac{RT}{(1 - \nu_2\rho)} \frac{s^{\circ}_{20,w}}{D^{\circ}_{20,w}}$$

where ρ is the density of the buffer and ν_2 is the partial specific volume of the protein, which were computed from the amino acid sequence using Sednterp.[31] The frinctional ratio, f/f_o, was computed from the following two relationships:

$$f = M_2 \frac{(1 - \overline{\nu}_2\rho_o)}{N s_{20,w}}$$

and

$$f_o = 6\pi\eta_o \left[\frac{3M_2(\nu_2 + \delta_1 \overset{\circ}{\nu}_1)}{4N\pi} \right]^{1/3}$$

where the symbols have their usual meaning.

AFM Sample Preparation and Imaging. For sample deposition, a specially modified mica surface (APS mica) was prepared by incubation of freshly cleaved mica in 167 μM 1-(3-aminopropyl)silatrane as previously described.[32−34] hSLIP1, hSLBP, and hSLBP−hSLIP1 complex samples were deposited on the APS mica immediately after dilution with PBS buffer. The sample concentrations were 8 and 24 nM for free hSLIP1 and SLBP, respectively, and 2−8 nM for the complexes. Samples were incubated on the APS mica surface for 2 min, washed with deonized water (AquaMax Ultra, LabWater.com), and dried in a stream of argon gas. All AFM images were acquired in air using a MultiMode AFM NanoScope IV system (Veeco/Bruker Instruments, Santa Barbara, CA) operating in tapping mode. Regular tapping mode silicon probes (Olympus, Asylum Research, Santa Barbara, CA) with a spring constant of ∼42 N/m and a resonance frequency between 300 and 320 kHz were used. Volume analysis was performed using the enum tool in FemtoScan [Advanced Technologies Center, Moscow, Russia (http://www.nanoscopy.net/manual/en/node116.html). Protein volumes were converted into masses (in kilodaltons) based on the conversion coefficient of 1.3 obtained from the volume measurement for proteins with known molecular masses as described previously.[35] The data were summarized as histograms using OriginLab (OriginLab Corp., Northampton, MA).

Surface Plasmon Resonance (SPR). Kinetic SPR studies were performed on a Biacore X instrument. A biotinylated hSLBP antibody was made toward the C-terminal 13 amino acids of hSLBP and was immobilized on a Biacore SA (streptavidin) sensor chip. Approximately 50−60 response units (RUs) was loaded onto the chip. Baculovirus-expressed phosphorylated SLBP was bound to the antibody and the RUs monitored as they reached the expected R_{max}. The chip was primed in BiaCore HBS-P buffer [10 mM Hepes (pH 7.4), 150 mM NaCl, and 0.005% Surfactant P20]. The hSLIP1 analyte concentrations were in the range of 1−50 μM, and all samples were prepared by dialyzing the hSLIP1 and hSLBP stock solutions against HBS-P buffer for 8−12 h. For determination of hSLBP−hSLIP1 binding kinetics, 120 μL of either wild-type or mutant hSLIP1 was injected onto the chip in the association phase at a flow rate of 30 μL/min followed by a 10 min dissociation phase during which only HBS-P buffer was injected. The bound protein was removed by short 20 s injection bursts of 3 M NaCl to restore the baseline. At least four or five sensorgrams were collected with varying protein concentrations. The data were analyzed using BiaEvaluation version 3.0. The control channel was subtracted; the sensorgrams were aligned, and the data for four or five sensorgrams were globally fit by least-squares analysis to a 1:1 Langmuir binding model. Both the association and dissociation phases were fit simultaneously. The best fit of the data was determined by the randomness of the residuals and the lowest value of χ^2 (goodness of fit) obtained. At least two independent sets of measurements were performed for each protein.

Computational Prediction of Protein−Protein Interaction Sites on SLIP1. To identify putative hot spots of interaction on hSLIP1 for hSLBP, we used the MIF4Gdb crystal structure as an input into Consurf (http://consurf.tau.

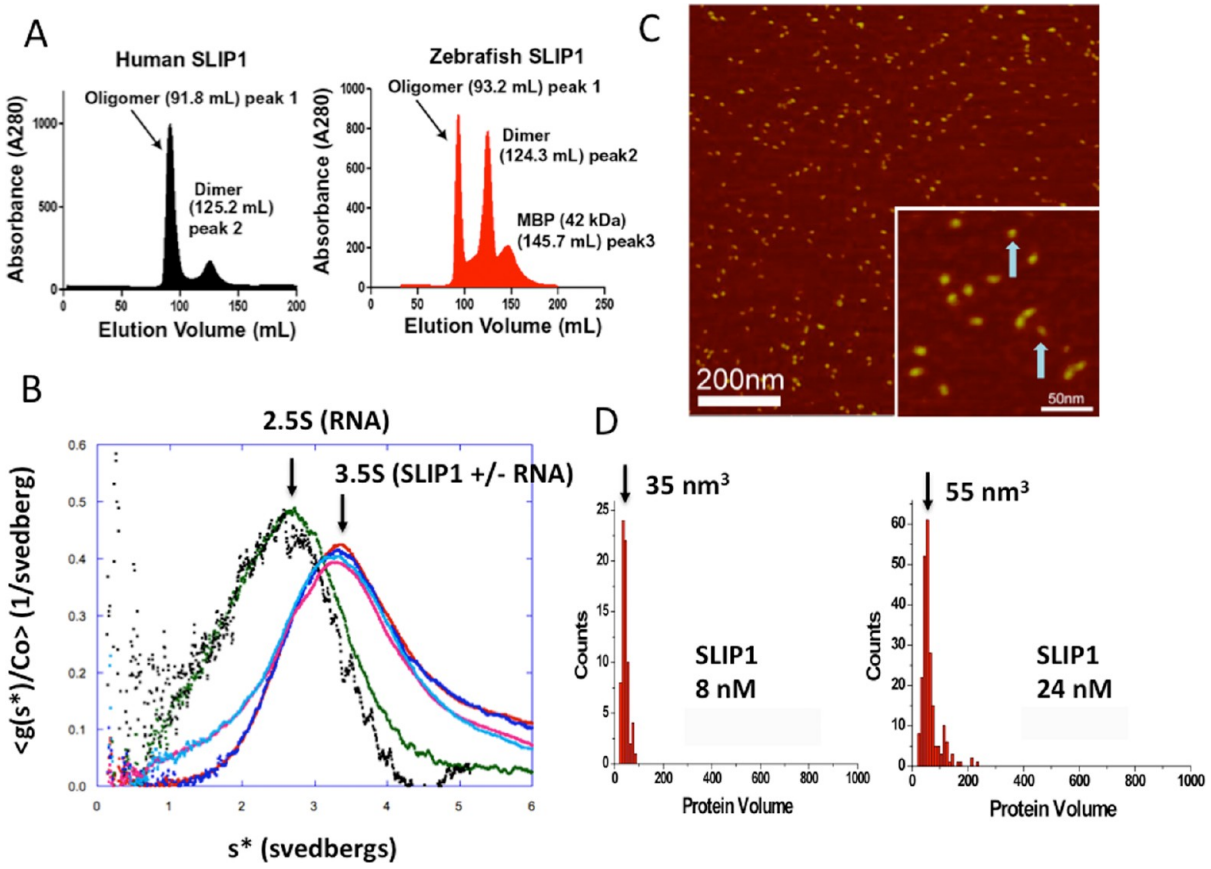

Figure 1. Human SLIP1 is a novel homodimer that does not bind RNA. (A) Gel filtration profiles for hSLIP1 and the zebrafish orthologue called MIF4Gdb on an S200 column (GE). hSLIP1 and MIF4Gdb migrate as higher-order oligomers as well as at the apparent molecular mass of the dimer (M_r ~ 52 kDa). (B) Sedimentation velocity profiles of hSLIP1 in the absence and presence of RNA. The samples were dialyzed against 10 mM potassium phosphate buffer (pH 7.4), 140 mM NaCl, and 2.7 mM KCl. For each sample, two different concentrations are shown (0.5 and 0.17 mg/mL). Sedimentation velocity profiles for hSLIP1 samples in the presence of a 2-fold molar excess of the histone mRNA stem–loop are colored cyan and pink. (C) AFM images of hSLIP1 at 24 nM. Blue arrows point to the two monomers. The hSLIP1 dimers are elongated in shape. (D) Histograms summarizing the volume measurements for the unbound hSLIP1 protein at 8 and 24 nM. For the 8 nM sample, N = 80 and bin size = 10. A conversion coefficient of 1.3 was used for globular proteins, which gave the monomer molecular mass of 27 kDa, corresponding to the SLIP1 monomer. For the 24 nM sample, N = 224 and bin size = 10.

ac.il/).[36] Consurf identifies functionally important regions on the surface of a protein with a known 3D structure based on phylogenetic relationships between homologues. We were particularly interested in identifying contiguous regions of highly conserved residues that were rich in charged or hydrophobic residues, because this is usually suggestive of a hot spot for protein–protein interactions. We also structurally aligned the MIF4Gdb structure with the available structures of yeast eIF4GI (PDB entry 2VSO) and human eIF4GII (PDB entry 1HU3). These structures superimpose with backbone root-mean-square deviations of 2.78 and 3.00 Å, respectively, and are most closely related to MIF4Gdb. This comparison allowed us to identify possible specificity-defining residues that occupied structurally similar positions in hSLIP1 and eIF4G but were different in sequence (Figure 7A and Figure 2 of the Supporting Information). hSLIP1 differs from eIF4GI and eIF4GII in the N-terminal HEAT repeats, whereas the C-terminal HEAT repeats are more closely related between these proteins. We also identified several residues toward the C-terminus of hSLIP1 that lie close to the dimer interface that preliminary small angle X-ray scattering (SAXS) data collected with an SLBP peptide (data not shown) suggested could be a possible interaction site for SLBP.

Circular Dichroism. All CD experiments were conducted at 25 °C using a JASCO J-815 CD spectrometer. The concentrations of SLIP1 and the SLIP1–SLBP complex were 5 μM in 20 mM sodium phosphate buffer (pH 7.0).

Additional methods are reported in the Supporting Information.

RESULTS

Human SLIP1 Forms a Novel Homodimer. The 1.92 Å crystal structure of MIF4Gdb (PDB entry 2I2O) is a crystallographic dimer and shows burial of an extensive interface of 888 Å^2 with 21 polar and nonpolar residues from each monomer contributing to dimer formation via electrostatic and hydrophobic interactions, respectively (Figure 1B of the Supporting Information). The homodimer is unique to MIF4Gdb and is absent from other proteins in the MIF4GD family, all of which exist as monomers. We sought to determine whether hSLIP1 exhibited biophysical properties similar to those of MIF4Gdb and if the two proteins were also dimeric in solution by gel filtration and analytical ultracentrifugation (Figure 1A,B and Table 2 of the Supporting Information). hSLIP1 and MIF4Gdb are both dimeric at concentrations of >1 mg/mL. When a concentrated solution (>20 mg/mL) of

dx.doi.org/10.1021/bi301074r | Biochemistry 2013, 52, 520–536

hSLIP1 or MIF4Gdb is loaded onto a Sephacryl 200 column, a substantial portion of the protein self-associates and elutes in the void volume. A fraction of the hSLIP1 and MIF4Gdb proteins elute as homodimers based on the elution volume and the sedimentation coefficient *s*-value (Figure 1A,B).

Oligomeric and RNA Binding Properties of hSLIP1 at Physiological Concentrations. To determine if hSLIP1 forms a dimer at physiologically relevant concentrations, we subjected the hSLIP1 sample to sedimentation velocity by analytical ultracentrifugation (AUC) analysis and AFM imaging. We used sedimentation velocity to determine the hydrodynamic parameters of hSLIP1 in the presence and absence of the 26-nucleotide histone mRNA stem–loop RNA (Figure 1B). Gel filtration fractions corresponding to the hSLIP1 dimer were dialyzed extensively against PBS buffer before the samples were subjected to AUC. In a concentration range of 0.1–0.5 mg/mL (~10 μM) (Figure 1B), the hSLIP1 sample showed the main peak was at an $s_{20,w}$ of 3.62, independent of concentration (Table 1). That value combined with a molar mass of 54414 g/mol, a partial specific volume of 0.733 cm^3/g, and a hydration value of 0.38 g/g, derived from the amino acid composition, gives an f/f_o value of 1.22 due to shape alone. This corresponds to a prolate ellipsoid having an axial ratio of 4.6, a length (hydrated) of 159.4 Å, and a diameter of 34.7 Å. These dimensions are consistent with hSLIP1 forming an elongated rodlike shape similar to that observed for MIF4Gdb. Sedimentation velocity patterns revealed some protein sedimenting at *s** ~5.7 S and some at higher *s*-values, consistent with hSLIP1 forming higher-order non-reversible aggregates at 0.5 mg/mL. Varying the concentration over a 27-fold range had no effect on the shape or position of the boundary. The addition of a 2-fold molar excess of histone mRNA stem–loop had no effect on the sedimentation coefficient, and the observed *s*-value for the mixture (hSLIP1 dimer + RNA) was that of the sum of hSLIP1 and RNA alone, indicating that the hSLIP1 dimer did not bind RNA (Figure 1B). This was confirmed by gel retardation or electrophoretic mobility shift assay (EMSA) experiments as discussed below (Figure 6E).

Table 1. *s*-Values and Molecular Masses of Proteins and RNA Measured by Analytical Ultracentrifugation at 20 °C

molecule	*s*-value[a] (S)	expected molecular mass (Da)
wild-type hSLIP1	3.4	54414
wild-type hSLIP1 with RNA	3.4	54414
R202A SLIP1	3.36	54244
R202A with RNA	3.17	54244
E200A SLIP1	2.5	27149
E200A SLIP1 with RNA	1.4	unfolded
hSLIP1–SLBP	6.7	116986
histone stem–loop RNA	2.5	8911

[a]Errors are ±0.01 S in this range.

We also examined the concentration dependence of dimer formation by AFM (Figure 1C,D). AFM allows one to examine the structural features of a macromolecule at nanometer resolution. An image of the hSLIP1 protein deposited on the APS mica surface at 24 nM is shown in Figure 1C. The shape of the protein molecules is uniform; the protein appears to be slightly elongated, which is consistent with the crystal structure of MIF4Gdb. The measured AFM volume for hSLIP1 is 55 nm^3. However, at a concentration of 8 nM, the protein volume decreases to 35 nm^3 (Figure 1D). Using the conversion coefficient for AFM volume measurements,[35] we conclude that at this concentration hSLIP1 is a monomer, suggesting that the monomer–dimer equilibrium exists in this concentration range. No evidence of the formation of large aggregates at these nanomolar concentrations is observed.

The N-Terminal Domain of hSLBP Is Intrinsically Disordered in Solution. To date, full-length hSLBP has not been characterized structurally or biophysically because it is difficult to express in bacteria. Functional studies have shown that sequences in the SLBP N-terminal domain [residues 1–110 (hSLBP-ND)] are important for translation initiation of histone mRNAs,[5] SLBP degradation,[37] and cyclin binding.[37] This region has also been proposed to be the binding site for hSLIP1.[12] Recombinant hSLBP-ND was expressed for structural characterization by NMR spectroscopy. Figure 2A shows ^{1}H–^{15}N HSQC spectra for uniformly ^{15}N-labeled human SLBP-ND recorded at 600 MHz. The spectra are characterized by a narrow chemical shift dispersion of ~1 ppm in the amide proton region over a pH range of 4–8 that is typical of either intrinsically disordered proteins[38] or coiled coils.[39] NMR spectra of coiled coils such as leucine zippers are infamous for the lack of chemical shift dispersion in the amide proton region.[40] To distinguish between these possibilities, we collected 2D and 3D NOESY data and made ^{15}N relaxation measurements. Only 89 of 123 expected amide resonances are observed in the ^{1}H–^{15}N HSQC spectra of hSLBP-ND recorded at 600 MHz (Figure 2A), with additional resonances of weak intensity appearing at 700 MHz with a cryoprobe (Figure 2D). The intrinsically disordered nature of hSLBP-ND was confirmed by ^{15}N–^{1}H heteronuclear NOE data (Figure 2E) and the lack of medium- or long-range NOE connectivities in 2D NOESY data collected with a range of mixing times (75–300 ms) as well as a 75 ms 3D ^{15}N-edited NOESY spectrum (data not shown). The NOESY spectra show a paucity of cross-peaks, and few dNNs indicative of a helical polypeptide were present. We also expressed the W75A mutant of hSLBP-ND because wild-type hSLBP-ND is prone to aggregation at millimolar concentrations required for NMR analysis and the aggregation is attributed directly to Trp75. However, mutation of Trp75 to alanine did not appreciably affect the spectral characteristics of the ^{1}H–^{15}N HSQC NMR spectra, indicating that the spectral characteristics of hSLBP-ND are not due to aggregation and are intrinsic to the flexible nature of this domain in solution (Figure 2B,C). It was not possible to obtain unambiguous assignments for backbone amide and ^{13}C resonances for either hSLBP-ND or the hSLBP-ND W75A mutant using triple-resonance NMR data because of the missing cross-peaks.

We also characterized the backbone dynamics of the W75A SLBP-ND protein on the nanosecond and picosecond time scales by measuring the ^{15}N T_1 and T_2 relaxation rates as well as the ^{15}N–^{1}H heteronuclear NOE. The ^{15}N–^{1}H heteronuclear NOE is a good indicator of internal dynamics in a protein and ranged from −0.44 to 0.64, with the average value being 0.05 (Figure 2E). In contrast to the N-terminus of dSLBP,[41] where the lines are sharp and the relaxation rates are very long (^{15}N T_2 ranges from 123 to 719 ms), hSLBP-ND shows shorter relaxation times for all peaks (average ^{15}N T_2 of ~100 ms). Taken together, the collapse in amide ^{1}H^N NMR chemical shifts near random coil values (8.0–8.4 ppm), the lack of medium- and long-range NOEs, and the backbone relaxation times indicate that in the absence of bound targets such as

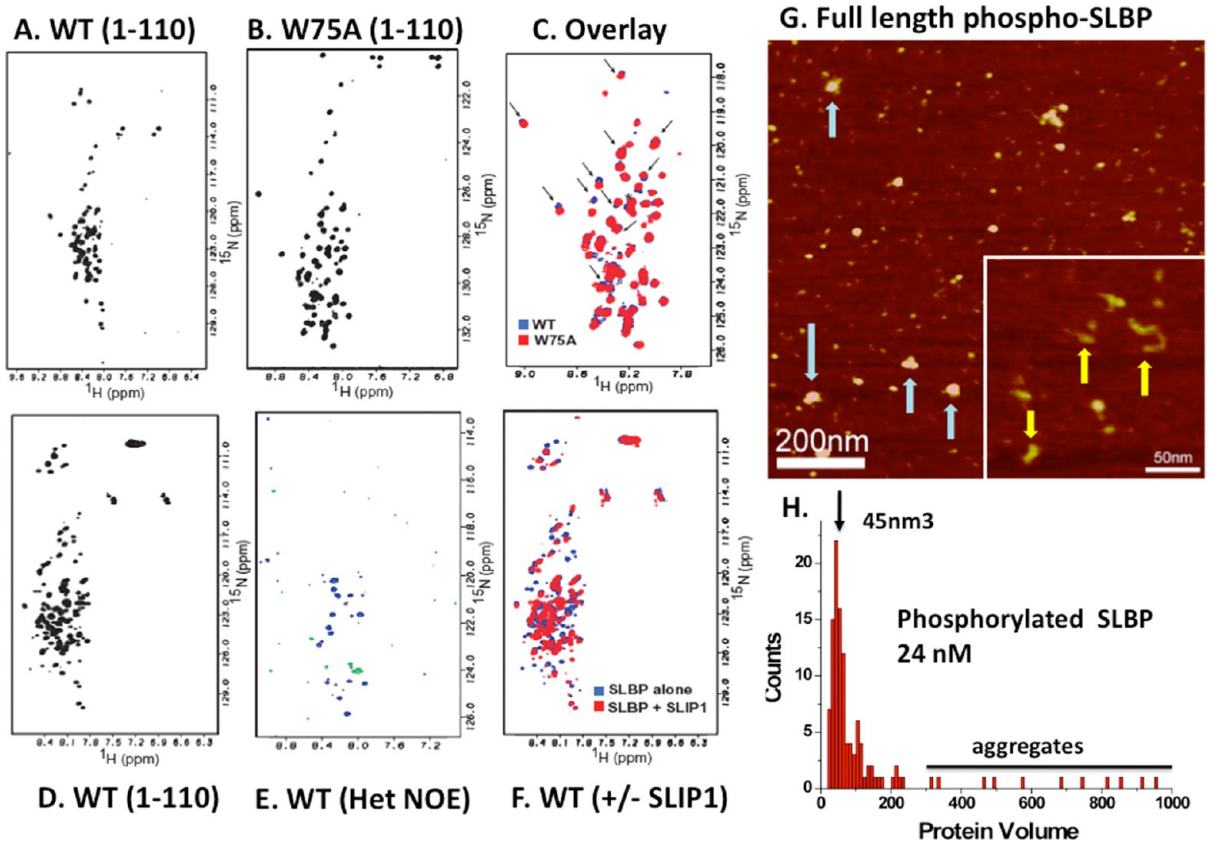

Figure 2. NMR and AFM characterization of human SLBP. (A) ^{1}H−^{15}N HSQC spectrum of the translation activation domain of hSLBP-ND collected at 600 MHz, pH 6.0, and 25 °C. (B) ^{1}H−^{15}N HSQC spectrum of the hSLBP-ND W75A mutant collected under the same conditions used for panel A. (C) Overlay of the WT (blue) and W75A mutant (red) spectra. (D) ^{1}H−^{15}N HSQC spectrum of human SLBP-ND WT collected at 700 MHz with a cryoprobe. Several additional peaks of low intensity appear at higher field. (E) {^{1}H}−^{15}N heteronuclear NOE spectrum collected with NOEs. Positive NOEs are colored blue and negative NOEs green. (F) ^{1}H−^{15}N HSQC spectrum of hSLBP-ND in the presence of an equimolar amount of hSLIP1 collected at a frequency of 600 MHz at 25 °C and pH 6.0. (G) AFM image of full-length baculovirus expressed hSLBP at 24 nM. Blue arrows point to the aggregates in the sample. The hSLBP monomers that are unstructured or partly structured are shown in the inset. Yellow arrows point to partially unstructured monomers. (H) Histogram summarizing the volume measurements for the unbound structured component of hSLBP protein at 24 nM. For the 24 nM sample, N = 118 and bin size = 10.

hSLIP1, the N-terminal domain (residues 1−110) of human SLBP does not adopt a stable fold in solution.

The hSLBP N-Terminal Domain (residues 1−110) Interacts Weakly with hSLIP1. To determine whether hSLBP-ND could independently bind hSLIP1, we performed NMR chemical shift perturbation experiments. Unlabeled hSLIP1 dimer (~54 kDa, at natural isotopic abundance) was titrated into a solution of uniformly ^{15}N-labeled hSLBP-ND (~12 kDa), and the changes the hSLBP-ND NMR resonances were recorded by collecting a series of ^{1}H−^{15}N TROSY spectra at 700 MHz in response to increasing amounts of hSLIP1 dimer added (Figure 2F and Figure 3 of the Supporting Information). Such chemical shift NMR mapping experiments are well-established in the literature and can provide important information about the binding site, the affinity, and the specificity of the interaction depending upon the chemical exchange regime being sampled by NMR.[42,43] To follow the effects of binding of hSLIP1 to hSLBP-ND in solution, we collected a series of ^{1}H−^{15}N TROSY spectra for which the hSLBP-ND concentration was held constant (0.2 mM) and the amount of hSLIP1 dimer was increased from 0 to 2.2 molar equivalents. Titration of substoichiometric amounts of hSLIP1 dimer (up to 0.5 equiv) into a solution of ^{15}N-labeled hSLBP-ND resulted in differential broadening of a subset of cross-peaks (21 peaks) in the ^{1}H−^{15}N TROSY spectrum (Figure 3 of the Supporting Information). Most of the remaining cross-peaks did not change their chemical shifts and showed a smaller change in peak intensity under these conditions. The observed decrease in peak intensity for the fraction of cross-peaks likely results from the "intermediate" chemical exchange regime on the NMR time scale expected for a low-affinity complex we estimate from SPR measurements (see below). In general, peak broadening is observed for weakly interacting systems (in either fast or intermediate exchange) where the K_d > 10 μM. Under these conditions, there would be an averaging of the line widths of hSLBP-ND resonances in the presence and absence of hSLIP1, and this effect will be experienced by resonances that are part of the hSLBP−hSLBP binding site. The disappearance of ~21 peaks in the beginning of the titration is consistent with previous mutagenesis studies that proposed only a 15 amino acid region in hSLBP-ND was important for translation activation[5] and hSLIP1 binding.[12] In the presence of a >1.5-fold molar excess of the hSLIP1 dimer, an overall broadening was observed due to the large molecular weight of the resulting complex (M_r ~ 78 kDa) that has a long rotational correlation time, and hence, there was a general loss of intensity of almost all peaks in the spectrum. These spectral changes are likely due to binding of the two proteins because the addition of 0.5 M

dx.doi.org/10.1021/bi301074r | *Biochemistry* 2013, 52, 520−536

NaCl to the complex reversed the effects and we were able to recover the spectrum of hSLBP-ND. Therefore, the interaction of the isolated N-terminal domain with hSLIP1 is weak, and the electrostatic effect of a high salt concentration can modulate the interaction.

Baculovirus-Expressed Human SLBP Is Phosphorylated at 23 Unique Ser/Thr/Tyr Sites. To determine whether the properties of the N-terminal domain were also reflected in full-length hSLBP, we expressed full-length hSLBP in baculovirus. As mentioned earlier, full-length hSLBP proteins cannot be expressed in bacteria as they are rapidly degraded and susceptible to proteolytic degradation. Because the baculovirus-expressed hSLBP protein is known to be phosphorylated at multiple sites,[37,44] we first characterized the phosphorylation state and the degree of chemical heterogeneity in baculovirus-expressed hSLBP using high-resolution LC−MS/MS along with a phosphopeptide enrichment method as described in Experimental Procedures. To identify all possible sites of phosphorylation, we used a bottom-up analysis approach using both tryptic and Glu-C peptide digests of hSLBP. This approach allowed us to obtain 85.2% coverage of the hSLBP sequence (Figure 3D), with multiple peptides that showed enrichment of the same phosphorylation sites. All phosphopeptides were detected with a very high mass accuracy and are summarized in Figure 3E and Table 3 of the Supporting Information. The assignments were manually validated via MS/MS fragmentation patterns. Panels A−C of Figure 3 show representative MS/MS spectra for the C-terminal S270-phosphorylated peptide that was identified using this approach. This analysis showed that when expressed in baculovirus, hSLBP is a hyperphosphorylated protein with at least 23 sites being phosphorylated (Figure 3E). We observed phosphorylation at Ser20, Ser23, Thr171, and Thr61 as previously reported,[37,44,45] although most of the sites we have identified herein are new and were not previously known. We identified 11 phosphorylation sites C-terminal to the SLBP RPD at Ser220, Ser221, Ser222, Thr226, Ser277, Ser278, Tyr235, Ser236, Thr238, Ser247, and Ser270. We have previously confirmed that hSLBP is phosphorylated in HEK293 cells at Ser221, Ser222, and Thr226.[45] Because a baculovirus is a eukaryotic expression system, at least a subset of the sites we report here may be biologically relevant. Nevertheless, the mass spectrometry analysis showed that baculovirus-expressed SLBP is a chemically heterogeneous mixture of several phosphorylated species, thereby preventing a thorough biophysical characterization of free hSLBP using equilibrium methods.

Because AFM is a single-molecule method, we imaged baculovirus-expressed hSLBP to determine whether structural states that corresponded to partially disordered hSLBP could be detected. AFM analysis of baculovirus-expressed hSLBP showed that even at a concentration of 8 nM, hSLBP forms aggregates (Figure 2G), the number and size of which increase over a period of 1 week (L. S. Shlyakhtenko, unpublished observations). The hSLBP monomers at 8 nM were partially unstructured as evidenced in Figure 2G (inset) by the formation of filamentous protein segments. Such protein morphology is characteristic of IDP regions in proteins,[46] suggesting that the intrinsic disorder of the N-terminal domain characterized by NMR is consistent with AFM imaging of full-length hSLBP. However, a fraction of the protein did adopt a more compact shape that could be integrated. Volume measurements showed that the distribution of the structured

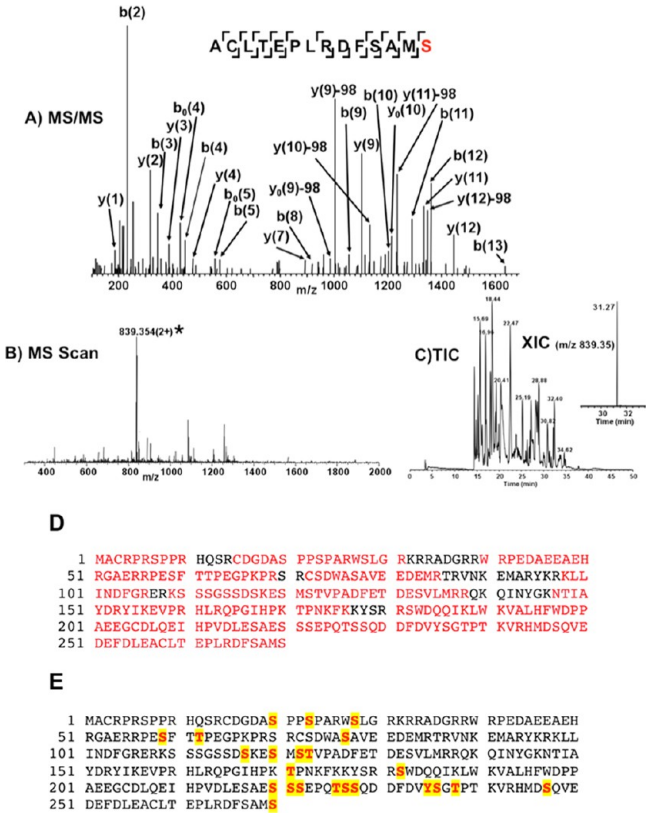

Figure 3. Mapping of phosphorylation sites in baculovirus-expressed full-length human SLBP by LC−MS/MS. (A−C) Identification of C-terminal phosphorylation in hSLBP by LC−MS/MS. Purified hSLBP was enzyme digested with Glu-C, followed by trypsin, prior to injection onto a C18 RP column attached to a NanoAquity UPLC system in line with a Hybrid Orbitrap Elite mass spectrometer. Peptides were separated over a 50 min linear gradient as shown in the total ion chromatogram (TIC) in panel C. The extracted ion chromatogram corresponding to the modified peptide is shown in the inset of panel C eluting in the 31 min region. (B) Collected high-resolution MS scan illustrating the exact mass (1676.6936 Da) determined for the modified peptide (asterisk). The subsequent MS/MS scan for the q-isolated modified peptide (asterisk) is presented in panel A, with corresponding b- and y-fragment ion series labeled. The site of fragmentation on the modified peptide backbone is represented by the top half-bracket and the bottom half-bracket for the y- and b-ions, respectively. (D) Total coverage (85.2%) of the observed phosphopeptides mapped onto the sequence of hSLBP. The peptide coverage is colored red, whereas sequences that were not detected in the bottom-up approach are colored black. (E) Ser, Thr, and Tyr residues for which we conclusively identified phosphopeptides in baculovirus-expressed hSLBP mapped on the SLBP sequence and colored red and yellow.

hSLBP monomers (molecular mass of 32 kDa) is centered around 44−45 nm^3 (Figure 2H), close to ∼42 nm^3 that is expected for a 32 kDa protein (calculated from a conversion coefficient of 1.3). We conclude that the chemically heterogeneous full-length baculovirus-expressed phosphorylated hSLBP appears on the AFM images as a mixture of structured and unstructured conformations. Phosphorylation at several sites likely contributes to the structural heterogeneity we observe in the AFM analysis. The AFM data also confirm that hSLBP is prone to aggregation, which is a characteristic feature of a number of IDPs.[47,48]

dx.doi.org/10.1021/bi301074r | *Biochemistry* 2013, 52, 520−536

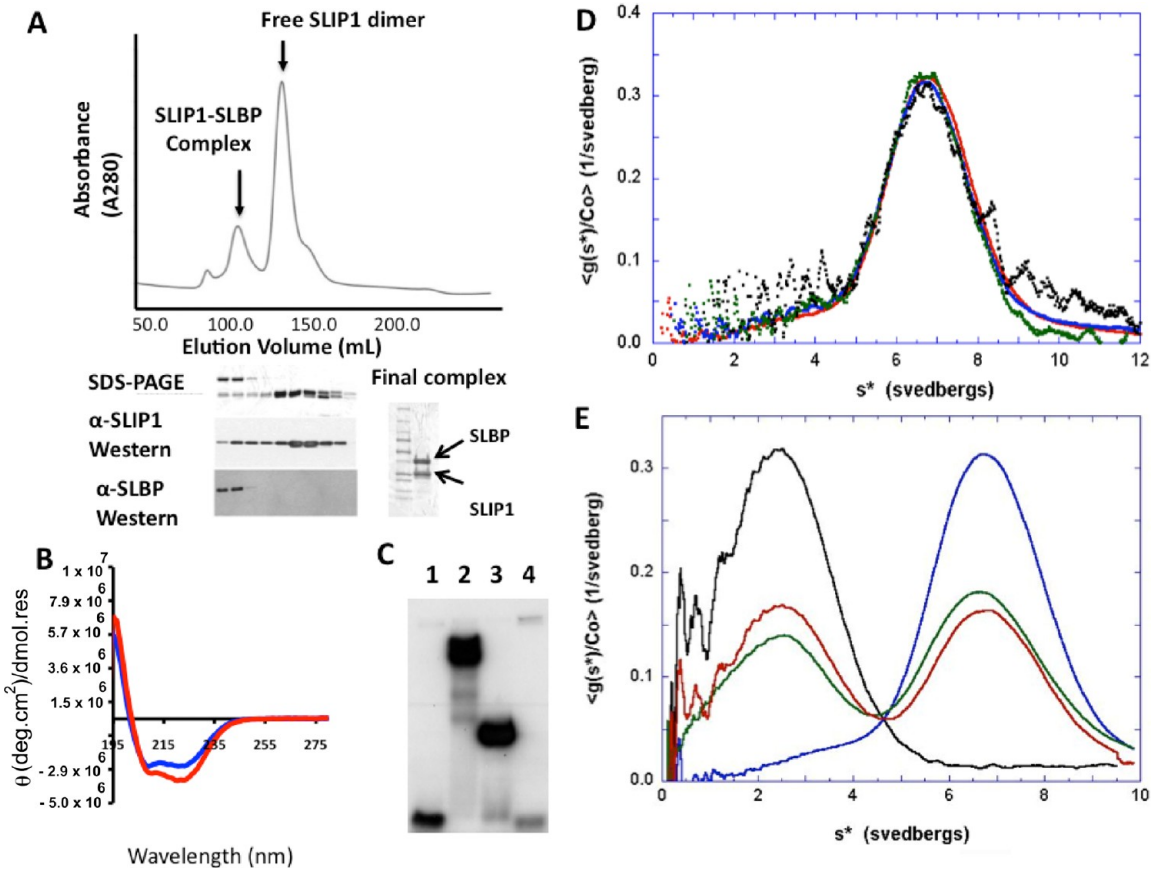

Figure 4. Biophysical characterization of the unphosphorylated hSLBP–hSLIP1 complex. (A) Gel filtration profile of the hSLBP–hSLIP1 complex copurified in the bacterial expression system after nickel affinity chromatography as the initial step. The SDS–PAGE gel of the corresponding fractions is shown. The apparent molecular mass of SLBP on a 4 to 20% SDS–PAGE gradient gel is ~37 kDa, and that of hSLIP1 is 26 kDa. The presence of hSLBP and hSLIP1 was confirmed by Western blotting using antibodies specific for the two proteins. hSLBP is present only in the first peak corresponding to the complex, whereas hSLIP1 is present in all fractions. The final concentrated sample of the complex shows a stoichiometric amount of hSLBP and hSLIP1. (B) Circular dichroism (CD) spectra of 5 μM free SLIP1 dimer (blue) and the HSLBP–hSLIP1 complex (red). The CD spectrum of free SLIP1 dimer shows double minima at 209 and 222 nm that are typical of helical secondary structure in proteins. There is an increase in the magnitude of the helical signal in the complex that could correspond to increased helical character of hSLBP in the complex. (C) Gel retardation experiment (EMSA) comparing the binding of full-length baculovirus-expressed SLBP (lane 2), the SLBP RNA binding and processing domain (lane 3), and the bacterially expressed and purified hSLBP–hSLIP1 complex (lane 4) shown in panel A. The free probe that is ^{32}P-labeled at the 5′ end is shown in lane 1. (D) Sedimentation velocity profiles of the hSLIP1–hSLBP complex shown in panel A at four different concentrations [0.20 (red), 0.10 (blue), 0.03 (green), and 0.01 mg/mL (black)]. No concentration-dependent change in the normalized sedimentation patterns was observed, demonstrating that there is no dissociation of the complex over this concentration range. (E) Sedimentation velocity profiles of the free histone stem–loop RNA (black), the hSLIP–hSLBP complex (blue), the hSLIP1–hSLBP complex with a 2-fold molar excess of histone stem–loop RNA (green), and the renormalized sum of the curves for free RNA and the hSLIP1–hSLBP complex (red), demonstrating that there is no interaction between the RNA and the complex under these conditions.

The Unphosphorylated Full-Length hSLBP–hSLIP1 Complex Forms a High-Affinity Heterotetramer That Is Impaired in Histone mRNA Binding. To characterize the structural and biophysical properties of the hSLBP–hSLIP1 complex, we co-expressed the two proteins in bacteria. We expressed full-length hSLBP as well as hSLBP-ND in a co-expression system in which only hSLIP1 was $(His)_6$-tagged. Full-length hSLBP formed a very stable complex with hSLIP1 and was copurified with hSLIP1 over a nickel affinity column as well as a gel filtration column (Figure 4A). The proteins form a stoichiometric complex as visualized by sodium dodecyl sulfate–polyacrylamide gel electrophoresis (SDS–PAGE) and were confirmed by Western blotting (Figure 4A). However, we could not form a stable complex with hSLBP-ND, the putative site of interaction with hSLIP1,[12] indicating that contrary to previous reports that suggest the N-terminal domain is sufficient for hSLIP1 binding,[12] there are additional sequence determinants for complex formation that lie between residues 111 and 270 of hSLBP. This is consistent with results from the NMR chemical shift mapping experiments discussed above, indicating that the interaction between the N-terminal domain and hSLIP1 is of weak affinity. The elution profile over a gel filtration column suggests that two monomers of hSLBP bind one dimer of hSLIP1 yielding an apparent molecular mass of ~110 kDa by gel filtration, which is close to the expected molecular mass of the heterotetramer of 116 kDa. The circular dichroism (CD) spectra of free hSLIP1 and the hSLBP–hSLIP1 complex (Figure 4B) confirm the helical secondary structure of hSLIP1, and an increase in the magnitude of the CD signal at 222 nm for the complex suggests that complex formation may induce helical structure, possibly in hSLBP.

We next analyzed the hydrodynamic properties of the hSLBP–hSLIP1 complex by AUC. The main peak in the sample showed an *s*-value of 6.7 S with a corresponding molar

dx.doi.org/10.1021/bi301074r | *Biochemistry* 2013, 52, 520–536

mass obtained by curve fitting of ~125 kDa (Figure 4D). This is close to a species consisting of two hSLIP1 monomers and two SLBP monomers (theoretical molar mass of ~116 kDa), indicating that the complex was a heterotetramer. Additionally, there was some evidence of the presence of a species at ~250 kDa (a dimer of the species at 125 kDa) as well as a species at ~50 kDa that could be a slight excess of the hSLIP1 homodimer or the hSLBP–hSLIP1 heterodimer. Statistical analysis also suggested that the observed $s_{20,w}$ value of 6.93 S (corrected) would be consistent with a mostly globular structure of the heterotetramer. That value combined with a molar mass of 116986 g/mol, a partial specific volume of 0.724 cm^3/g, and a hydration value of 0.417 g/g, derived from the amino acid composition, gives an f/f_o value of 1.1. The corresponding hydrated sphere would have a sedimentation coefficient value of ~7.60 S, and therefore, the heterotetramer would have an f/f_o frictional ratio due to shape alone of 1.10. This corresponds to an ellipsoid of revolution with an axial ratio of ~2.8 using the Perrin equation, a typical value for nearly globular proteins. If the protein were modeled as a prolate ellipsoid, the expected length (hydrated) would be 148.2 Å and the diameter 53.5 Å. The prediction of a globular complex in solution as well as the tetramer species obtained by sedimentation velocity was confirmed by AFM images (Figure 6A, inset). Altogether, AFM images revealed the existence of four different species in the sample. Two small protein volumes of 35 and 55 nm^3 likely represented the free hSLIP1 monomer and the hSLIP1 dimer, respectively, and protein volumes of 85–90 nm^3 likely corresponded to the hSLBP–hSLIP1 heterodimer (estimated volume of ~75 nm^3). The heterotetramer has a protein volume of 165 nm^3, well within the range expected for a molecular mass of 116 kDa (expected volume of ~151 nm^3).

When the concentration dependence of the sedimentation velocity profile was tested down to 85 nM, no dissociation of the hSLBP–hSLIP1 complex was observed (Figure 4D). This indicates that the complex is remarkably stable with a K_D value estimated to be less than 0.9 nM. This is a surprising result and indicates that residues 111–270 (the RNA binding domain and additional C-terminal residues) participate in formation of the heterotetramer. To determine whether the RNA binding domain was capable of forming a dimer, we collected mass spectrometry data on the unphosphorylated bacterially expressed hSLBP RNA binding domain as well as the phosphorylated baculovirus-expressed RNA binding domain. When expressed in baculovirus, the hSLBP RBD is phosphorylated at only one site, a conserved threonine (Thr171) in the TPNK sequence.[44,49] Phosphorylation at Thr171 is important for the kinetics of histone mRNA binding by SLBP.[49] The unphosphorylated hSLBP RBD mass spectrum clearly showed evidence of strong monomer (32.7%) and dimer (35.3%) peaks (almost equimolar), and smaller peaks were also observed for the trimer, tetramer, and hexamer (Figure 5A). The monomer, dimer, trimer, and tetramer species are also present in the mass spectrum of the phosphorylated baculovirus-expressed RBD; however, the monomer species predominated (86.6%), and only 5.6% mass corresponded to the dimer, 3.9% to the trimer, and 3.8% to the tetramer (Figure 5B). Therefore, the hSLBP RBD tends to self-associate, and this association is enhanced when the protein is not phosphorylated at Thr171 in its RNA binding domain.

To test whether the unphosphorylated hSLBP–hSLIP1 complex could bind the histone mRNA stem–loop structure,

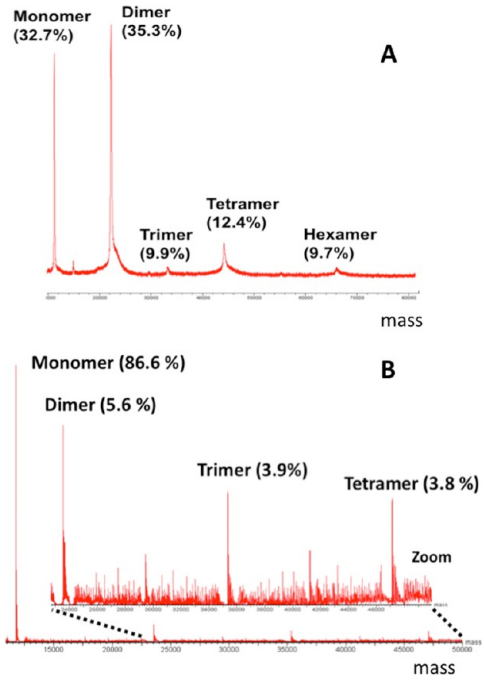

Figure 5. Analysis of the phosphorylated and unphosphorylated SLBP RNA binding and processing domains (RPD) by mass spectrometry. (A) MALDI-TOF mass spectrum of the bacterially expressed unphosphorylated hSLBP RPD. The monomer:dimer:trimer:tretramer:hexamer mass ratio obtained from the peak intensities was 32.7:35.3:9.9:12.4:9.7. (B) Electrospray mass spectrum (ES-MS) of the phosphorylated hSLBP RBD obtained on a Qtof-Micro mass analyzer. The mass obtained was 11783.00 Da, corresponding to a single phosphate at Thr230, cleavage of the N-terminal Met, and acetylation of the N-terminal serine. On the basis of peak heights, the monomer:dimer:trimer:tetramer ratio was 86.6:5.6:3.9:3.8.

we added up to 2 molar equivalents of RNA. The sedimentation profile observed for the mixture (hSLBP–hSLIP1 complex + RNA) was essentially the same as that for the sum of the patterns seen for RNA alone and the complex alone (Figure 4E). If the RNA caused the complex to dissociate, we would expect a shift in the main peak at 6.7 S to lower values. The main peak, corresponding to the complex, remained solidly at 6.7 S, and the peak at 2.5 S (the RNA) did not interact with the complex. The hSLBP–hSLIP1 complex and RNA behave as independent species. To confirm that the hSLBP–hSLIP1 complex did not interact with RNA, we performed EMSA or gel retardation experiments (Figure 4C). We formed a stable complex of ^{32}P-labeled histone stem–loop RNA with baculovirus-expressed phosphorylated full-length hSLBP (Figure 4C, lane 2) as well as the hSLBP RBD (Figure 4C, lane 3); however, no discernible shift of the labeled RNA probe was observed in the presence of the unphosphorylated hSLBP–hSLIP1 complex (Figure 4C, lane 4). Therefore, the interaction of the unphosphorylated full-length hSLBP with hSLIP1 results in an inactive heterotetramer that does not bind histone mRNA. The inability of the unphosphorylated hSLBP–hSLIP1 complex to bind RNA could be because the hSLBP RBD is auto-inhibited in the heterotetramer, hSLBP needs to be phosphorylated at Thr171 to bind RNA efficiently, or both. We have shown previously[44] that phosphorylation of the hSLBP RBD at Thr171 in the highly conserved TPNK sequence is important for formation of a stable complex with the histone mRNA stem–loop.

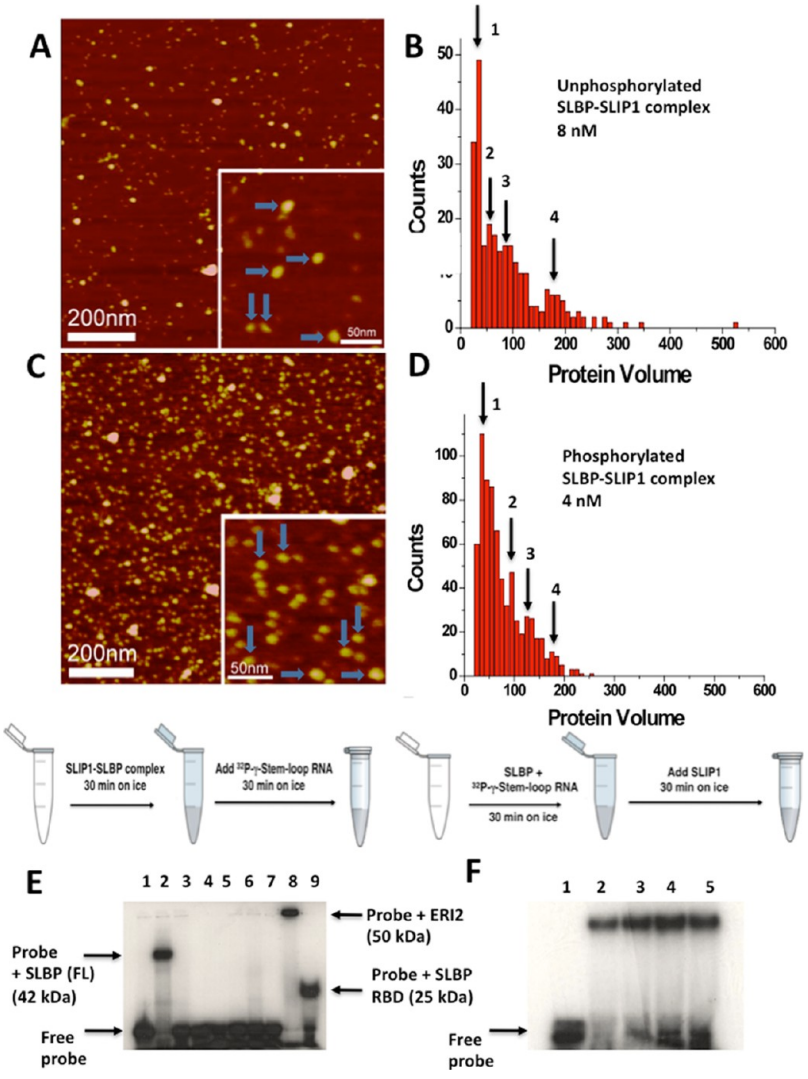

Figure 6. Analysis of the phosphorylated and unphosphorylated hSLBP–hSLIP1 binary and hSLBP–hSLIP1–histone mRNA ternary complexes by AFM and EMSA. (A) AFM image of the bacterially expressed unphosphorylated hSLBP–hSLIP1 complex at 8 nM. The horizontal blue arrows point to heterotetramers with protein volumes of around 180–200 nm^3. The vertical arrows point to heterodimers with a protein volume of around 90 nm^3. (B) Histogram summarizing the volume measurements for the complex in panel A. For the 8 nM sample, N = 272 and bin size = 10. (C) AFM image of the baculovirus-expressed phosphorylated hSLBP–hSLIP1 complex at 4 nM. The horizontal blue arrows point to heterotetramers with protein volumes of around 170 nm^3. The vertical arrows point to heterodimers with a protein volume of around 90 nm^3. The image shows an increase in the population of heterodimers relative to heterotetramers in the sample. (D) Histogram summarizing the volume measurements for the complex in panel C. The concentration of the protein was 4 nM; N = 700, and bin size = 10. The four maxima observed in panels B and D are summarized in Table 2. (E) EMSA of baculovirus-expressed hSLBP and hSLIP1. The schematic showing how the reaction was performed is shown above the gel. In all reactions, the histone mRNA probe was added last after the proteins had been incubated on ice for 30 min. The free histone mRNA stem–loop probe (final concentration of 0.1 nM) that is labeled at the 5′ end with [γ-^{32}P]ATP is shown in lane 1, and the interaction of full-length hSLBP (final concentration of 2 mM) with the histone mRNA probe is shown in lane 2. No interaction of hSLIP1 (final monomer concentration of 6 mM) with histone mRNA occurs in the absence (lane 3) or presence (lane 4) of 5 mM cross-linking agent (DSP). In lanes 5–7, hSLBP (2 μM) was incubated with increasing concentrations of hSLIP1 (12, 24, and 36 μM, respectively), and the reaction mixtures kept on ice for 30 min. This was followed by addition of the [γ-^{32}P]ATP histone stem–loop RNA for an additional 30 min. No interaction of either SLBP or the complex is observed. Lane 5 shows the interaction of 2 μM ERI2 exonuclease with histone stem–loop RNA (complex M_r ~ 50 kDa), and lane 6 shows the interaction of the hSLBP RBD with histone stem–loop RNA (complex M_r = 25 kDa). (F) EMSA showing the interaction of hSLBP with the histone mRNA stem–loop RNA followed by addition of increasing concentrations of hSLIP1. Lane 1 shows the free probe (0.1 nM), and lane 2 shows the probe complexed to hSLBP (2 μM). Lanes 3–5 show the interaction of the hSLBP–RNA complex with 12, 24, and 36 μM hSLIP1, respectively. The hSLIP1 protein was added to a preformed SLBP–RNA complex as depicted in the schematic above the gel.

Sequential and Ordered Assembly Is Required To Form the hSLBP–hSLIP1–Histone mRNA Complex. To form a phosphorylated hSLBP–hSLIP1 complex, we performed AFM on an equimolar mixture of phosphorylated baculovirus-expressed phosphorylated hSLBP and bacterially expressed hSLIP1 at nanomolar concentrations. When a 4 nM dilution of the complex solution was deposited on the mica surface, the volume measurements suggested that the hSLIP1 monomer (35 nm^3), the hSLBP–hSLIP1 heterodimer (95 nm^3), and the hSLBP–hSLIP1 heterotetramer (175 nm^3) were present (Figure 6C,D). To test whether the baculovirus-expressed phosphorylated hSLBP–hSLIP1 complex could form a ternary

dx.doi.org/10.1021/bi301074r | *Biochemistry* 2013, 52, 520–536

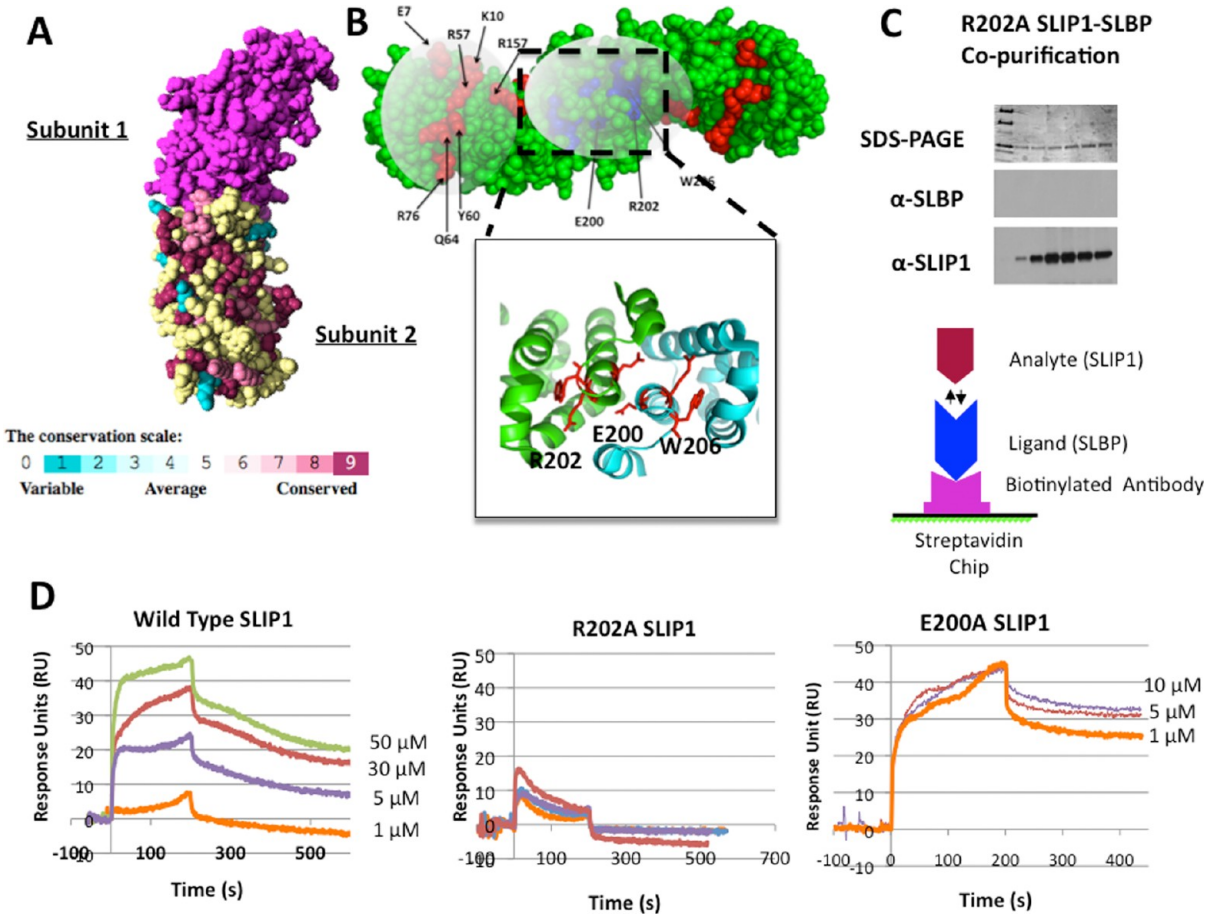

Figure 7. Mapping the binding site on hSLIP1 for hSLBP using computational prediction and Surface Plasmon Resonance (SPR). (A) The Consurf algorithm was used to predict hot spots for protein−protein interaction on the surface of MIF4Gdb (PDB entry 2I2O). The conservation of residues based on multiple-sequence alignment of hSLIP1 orthologues in eukaryotes is mapped onto subunit 2 of the MIF4Gdb homodimer. The conservation is shown on a 0−9 scale and is represented by surface coloring, which varies linearly from blue (variable) to magenta (highly conserved). Yellow suggests insufficient data. The sequence alignment of hSLIP1 orthologues is shown in the Supporting Information. (B) Ten of the 15 highly conserved residues selected for these studies are shown. Residues E7, K10, R57, Y60, Q64, R76, and R157 are highly conserved and may form one contiguous surface that could be a hot spot for hSLIP1-mediated protein−protein interactions. Residues E200, R202, and W206 form a second surface that lies close to the dimer interface (shown in the inset). Other residues that were selected and expressed but are not shown on the figure include H44, F75, F87, R82, and R93. (C) Copurification of the R202A SLIP1 mutant with full-length hSLBP was attempted. The panels in panel C show the SDS−PAGE gels after nickel chromatography showing only hSLIP1 protein bound the nickel column. The panels below show Western blots for hSLBP and hSLIP1 on the same fractions that confirm that no SLBP protein was present in the fractions that had hSLIP1. (D) Surface Plasmon Resonance sensorgrams are shown for the interaction of wild-type hSLIP1, R202A hSLIP1, and E200A hSLIP1 with hSLBP. The experimental design for the secondary capture method used is shown. A biotinylated SLBP antibody toward the C-terminal 13 amino acids of hSLBP was bound to a streptavidin chip. The ligand hSLBP was passed onto the chip until the change was no more than 50−60 RUs. The chip was washed with buffer; then the respective wild-type and mutant SLIP1 analytes were passed across the chip at a flow rate of 30 μL/min, and the change in the response was monitored. The sensorgrams for the wild type and R202A mutant are shown on the same RU scale. Four or five different hSLIP1 concentrations were used to fit the data.

complex with histone mRNA, we performed EMSA analysis two ways, as shown in panels E and F of Figure 6. In the absence of hSLIP1, hSLBP formed a high-affinity complex with the ^{32}P-γ-labeled histone mRNA stem−loop RNA as shown in lane 2 of Figure 6E, whereas the isolated hSLIP1 did not bind the histone stem−loop RNA in an EMSA in the absence (Figure 6E, lane 3) or presence (Figure 6E, lane 4) of the cross-linker dithiobissuccinimidylpropionate or DSP (Pierce). Full-length phosphorylated hSLBP bound the histone stem−loop RNA as a monomer, because the complex migrated between the hSLBP RBD−RNA complex [M_r = 25 kDa (Figure 6E, lane 9)] and the ERI2−histone mRNA complex [M_r = 50 kDa (Figure 6E, lane 8)]. Remarkably, when full-length phosphorylated hSLBP was mixed with increasing concentrations of hSLIP1 (Figure 6E, lanes 5−7) and the reaction mixture was incubated on ice for 30 min followed by addition of ^{32}P-labeled histone mRNA stem−loop RNA, no binding of hSLBP to the stem−loop RNA was observed, similar to that observed for the bacterially expressed unphosphorylated hSLBP−hSLIP1 complex. However, when hSLBP was incubated with the histone mRNA stem−loop RNA first, followed by the addition of hSLIP1, the hSLBP remained bound to the histone mRNA (Figure 6F) even in the presence of a 10-fold molar excess of hSLIP1. No evidence of a ternary histone mRNA−SLBP−SLIP1 complex was observed under these conditions. As we show below, phosphorylated (and monomeric) hSLBP interacts weakly with hSLIP1 with a K_D of ∼3 μM, and it is likely that the ternary complex (1:1:1 RNA−hSLBP−hSLIP1 complex)

dx.doi.org/10.1021/bi301074r | *Biochemistry* 2013, 52, 520−536

has a fast off rate and is not detected in a gel retardation experiment. This is an important result as it indicates that the assembly of the translation initiation complex requires prebinding of hSLBP to the histone mRNA as a monomer first, followed by interaction with hSLIP1. Taken together with previously published data on the effects of Thr171 phosphorylation on RNA binding[44,49] and the mass spectrometry data shown in Figure 5, our data suggest that phosphorylation of hSLBP in the RBD (at Thr171) facilitates interaction with histone mRNA and promotes disruption of the heterotetramer to preferentially form a 1:1:1 RNA−hSLBP−hSLIP1 complex.

hSLBP Binds hSLIP1 near the Homodimer Interface. Using the MIF4Gdb crystal structure as a guide, we mutated 15 residues in hSLIP1 that comprised two contiguous surfaces, as potential binding sites for hSLBP as described in Experimental Procedures (Figure 7B). Each residue was mutated to alanine, expressed in *E. coli*, and purified to homogeneity. We were able to express all single-site alanine mutants with the exception of W206A, which was severely destabilized and shuttled into inclusion bodies when expressed in *E. coli*. We established a Surface Plasmon Resonance (SPR) assay to study the interaction of hSLIP1 with baculovirus-expressed full-length phosphorylated hSLBP (Figure 7D). We used an indirect capture method in which the biotinylated hSLBP antibody (made toward the C-terminal 13 amino acids of hSLBP) was bound to a streptavidin chip (Figure 7). Baculovirus-expressed full-length hSLBP was bound to the antibody, and wild-type or mutant hSLIP1 proteins were passed onto the chip and the binding kinetics derived from the SPR sensorgrams. When low concentrations of the hSLBP−antibody complex are loaded onto the chip, the hSLBP ligand is expected to be a monomer. The experimental design allows a monomer of hSLBP to interact with either a monomer or a dimer of hSLIP1. The data showed that hSLIP1 binds the hSLBP monomer with a slow on rate and a moderate off rate (Figure 7D and Table 2), yielding a

Table 2. Rate Constants Derived from Surface Plasmon Resonance for Full-Length Baculovirus-Expressed Phosphorylated hSLBP toward hSLIP1 at 25 °C

hSLIP1 protein	k_{+1} (M^{-1} s^{-1})	k_{-2} (s^{-1})	K_D (μM)	K_D (rel)[a]
wild-type hSLIP1	634	2.38×10^{-3}	3.75 ± 1.8	
R202A hSLIP1	nd	nd	nd	>100
K10A hSLIP1	542	1.17×10^{-3}	2.15 ± 0.9	0.57
R76A hSLIP1	181	5.49×10^{-4}	3.02 ± 2.2	0.81
E200A hSLIP1	8310	5.49×10^{-3}	0.066 ± 0.02	0.0176
H44A hSLIP1	161	2.52×10^{-3}	15.6 ± 5.4	4.16

[a] K_D values representing K_D(mut)/K_D(wt), i.e., the interaction of mutant hSLIP1 relative to the wild-type hSLIP1 protein.

K_D of 3.75 μM. This K_D is orders of magnitude weaker than that observed for the bacterially expressed unphosphorylated hSLBP−hSLIP1 complex by AUC. The R202A mutation completely abrogated binding of hSLIP1 to hSLBP at the highest concentration tested (50 μM), whereas no appreciable change in affinity was observed toward a number of other mutants tested (Table 2). To confirm the inability of R202A hSLIP1 to bind hSLBP, we expressed full-length hSLBP in the same bacterial co-expression system as described earlier in which R202A hSLIP1 was $(His)_6$-tagged. No hSLBP copurified with R202A hSLIP1 after nickel affinity chromatography (Figure 7C). Surprisingly, the E200A hSLIP1 mutant showed a 10-fold increase in affinity toward hSLBP (Figure 7D and Table 2). The E200 residue lies at the hSLIP1 dimer interface, and in MIF4Gdb, this residue participates in a network of hydrogen bonding interactions. Sedimentation velocity data indicated that E200A hSLIP1 sediments at a lower *s*-value of 2.5 S and likely represents the hSLIP1 monomer (Figure 5C of the Supporting Information). Intriguingly, the addition of RNA resulted in unfolding of the E200A hSLIP1 protein, indicating that the protein is destabilized (Figure 5C of the Supporting Information). In contrast, the R202A hSLIP1 mutant sedimented with an *s*-value of 3.4S and did not bind RNA, like the wild-type hSLIP1 dimer (Figure 5B of the Supporting Information).

The R202A hSLIP1 Mutant Alters Histone mRNA Abundance in vivo. To investigate whether disruption of the hSLBP−hSLIP1 interaction observed in the R202A mutant affected histone mRNA expression, we transfected flag-tagged wild-type hSLIP1 and the R202A hSLIP1 mutant into HeLa cells. The expression of the mutant R202A protein (Figure 8B) was comparable to that of the wild-type exogenously transfected hSLIP1 protein. There was no change in the cell cycle distribution of HeLa cells due to overexpression of either wild-type or R202A hSLIP1 24 h after transfection (Figure 8D). However, 72 h after transient transfection, cells expressing wild-type or R202A hSLIP1 accumulated in the G1 phase of the cell cycle, and a reduction in the number of cells in the S phase of the cell cycle was observed. This effect was much more pronounced for the R202A mutant hSLIP1-expressing cells. hSLIP1 is an essential protein in eukaryotes, and knockdown of hSLIP1 by siRNA has been reported to result in cell death.[12] Consistent with this, we observed that significant (>50%) cell death occurred within 24 h of the treatment of the HeLa cells with an hSLIP1-specific siRNA. We were not able to rescue cell viability by cotransfection of siRNA resistant R202A or siRNA resistant wild-type hSLIP1. The ability to restore cell viability is reported to be siRNA-specific.[12] We also compared the cellular localization of the R202A hSLIP1 mutant to that of the endogenous wild-type hSLIP1 protein as well as the exogenous overexpressed wild-type hSLIP1 protein using CCD microscopy of HeLa cells (Figure 8A). To distinguish between S phase cells and cells in the G_1 and G_2 phases of the cell cycle, we pulse-labeled the transfected HeLa cells with the nucleoside analogue (5-ethynyl-2′-deoxyuridine or EdU) and immunolabeled the sites of EdU incorporation using the anti-EdU Alexa Fluor 488 secondary antibody. EdU is incorporated only into single-stranded DNA, and only S phase cells are labeled.[50] The spatial distribution of EdU containing fluorescent foci in the cell nucleus also allows one to distinguish between early S, middle S, and late S phase cells (A. Fritz and R. Berezney, unpublished results) as previously determined following bromodeoxyuridine incorporation.[50,51] The endogenous hSLIP1 protein is localized predominantly on the endoplasmic reticulum, consistent with its role in mRNA translation, and more diffuse staining was observed in the cytoplasm and nucleus. An interesting property of endogenous hSLIP1 is that although it does not appear to be regulated during the cell cycle, hSLIP1 is excluded from lipid vacuole-like structures in the cytoplasm particularly in cells that are in the late S stage of the cell cycle (Figure 8A and Figure 6 of the Supporting Information). The exogenously overexpressed wild-type and R202A hSLIP1 proteins were also expressed throughout the cell cycle and excluded from the lipid vacuoles. However, overexpression of both wild-type and R202A hSLIP1 resulted

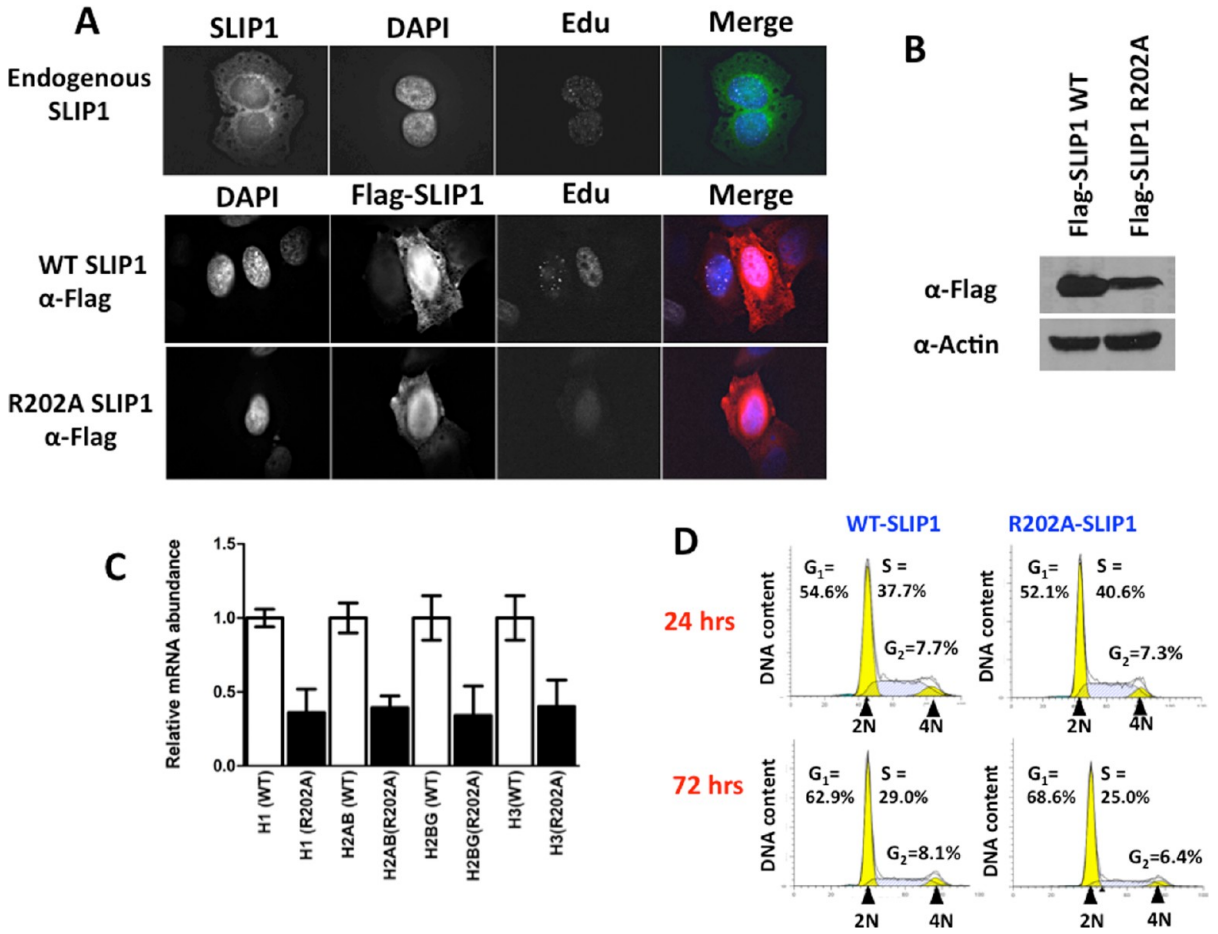

Figure 8. Characterization of the WT and R202A mutant hSLIP1 proteins in vivo. (A) Subcellular localization of endogenous hSLIP1 and exogenous wild type Flag-tagged hSLIP1 and the Flag-tagged R202A hSLIP1 mutant in HeLa cells was visualized in 0.5 μm optical sections using a CCD microscope and deconvolution system as described in the Supporting Information. HeLa cells were transiently transfected with Flag-tagged wild-type or mutant hSLIP1 as indicated. The cells were grown on coverslips, permeabilized, and pulse-labeled with EdU to stain for S phase cells and labeled with DAPI for nuclear imaging. hSLIP1 is colored red, DAPI blue, and EdU green. The first panel shows two cells in late S phase with endogenous hSLIP1 present predominantly on the endoplasmic reticulum. Diffuse staining indicates that some hSLIP1 is also present in the nucleus and in the cytoplasm. The second panel shows cells transiently transfected with wild-type hSLIP1. The cell is in middle S phase and shows mostly nuclear and some cytoplasmic staining. The third panel shows the localization of R202A hSLIP1. DAPI is colored blue and α-Flag-tagged hSLIP1 red. The individual staining patterns are also shown in Figure 6 of the Supporting Information. (B) Protein expression levels of transiently transfected Flag-tagged wild-type hSLIP1 and Flag-tagged R202A hSLIP1 used for the CCD microscopy and qPCR experiments. The cells were harvested 24 h after transfection and probed by Western blotting using an α-Flag antibody. (C) Real-time qPCR of histone genes in HeLa cells was performed to compare mRNA levels in cells transiently transfected with either wild-type hSLIP1 or R202A hSLIP1. The average fold change determined from the C_t values using the comparative C_t method is depicted with the standard errors derived from three independent data sets. Only one band was observed for all genes analyzed, and the primers were specific for the target genes being tested. The data were normalized to GAPDH. (D) hSLIP1 overexpression results in an increased level of accumulation of cells in the G_1 phase and a reduced level of accumulation in the S phase. Cell cycle profiles of HeLa cells transiently transfected with either wild-type or R202A hSLIP1. Cells were pulse labeled with propidium iodide, and the DNA content was analyzed by flow cytometry; the cell cycle distribution was determined using ModFit.

in more accumulation of hSLIP1 in the nucleus compared to endogenous hSLIP1 (Figure 8A). No difference was observed in the localization of the exogenous R202A hSLIP1 mutant compared to that of the exogenous wild type in vivo.

We compared the expression of histone mRNA in cells expressing R202A hSLIP1 and wild-type hSLIP1 by qPCR (Figure 8C). A significant reduction (by at least 60%) in the levels of the core histone mRNAs was observed in cells that overexpressed R202A hSLIP1 compared to cells that expressed wild-type hSLIP1, consistent with a role of hSLIP1 in regulation of histone mRNA metabolism. Because R202A hSLIP1 was expressed and localized in a manner similar to that used for wild-type hSLIP1, we attribute the decreased histone mRNA levels in the R202A hSLIP1 mutant-expressing cells to either an increased level of degradation or a decreased level of processing or export of the histone message caused by disruption of the hSLBP–hSLIP1 interaction. A more detailed functional characterization of the hSLIP1 R202A mutant is necessary to understand the mechanism by which it regulates histone gene expression. However, the biological data are consistent with our biophysical experiments that suggest that R202 is an important "hot spot" on hSLIP1 for interaction with SLBP.

DISCUSSION

The hSLBP–hSLIP1 complex is an example of a specific mRNA binding complex that assembles on the 3′-untranslated region of histone mRNA to regulate its translation. Despite the

dx.doi.org/10.1021/bi301074r | *Biochemistry* 2013, 52, 520–536

available biological data that implicate these proteins in bridging the 3′ end of the histone mRNA with the eIF4F complex on the 5′ end,[12,23] there is no structural information available about these proteins either free or complexed to each other or bound to RNA. We sought to establish two pieces of information from this study. First, our biophysical characterization of hSLIP1, hSLBP, and the hSLBP−hSLIP1 complexes using equilibrium and single-molecule methods has allowed us to describe a model for the overall architecture of the complex, the stoichiometries of hSLBP and hSLIP1, and how the complex may be activated by phosphorylation and oligomerization. Second, we have mapped the site of interaction of hSLBP with hSLIP1 using structural bioinformatics tools and biochemical experiments to gain insight into how the two proteins may associate in vivo to regulate histone gene expression.

Isolated hSLBP Is Intrinsically Disordered and Phosphorylated at Several Ser/Thr Sites. We have shown by NMR that hSLBP is an IDP.[52] The global disorder observed for the first 110 residues of the mammalian N-terminus described here was also observed previously for residues 1−175 of *Drosophila* SLBP.[41] hSLBP and dSLBP perform very similar functions in the cell; however, there is no sequence identity between the N-terminal domains of dSLBP and hSLBP, yet the lack of ordered structure appears to be important for their function. At least a third of eukaryotic proteins that participate in signaling and gene expression have intrinsically disordered regions of 30 or more residues.[53] Analysis of binding mechanisms for several IDPs shows that the increased conformational flexibility allows IDPs to interact with numerous targets, provides greater surface area for interaction, and facilitates better regulation of their function via posttranslational modifications.[54,55] Functional studies have shown that the N-terminal domain of hSLBP must interact transiently with numerous factors in the nucleus and the cytoplasm to regulate histone mRNA processing, export, translation, and degradation.[1] We speculate that the intrinsic disorder of the N-terminal domain may allow hSLBP to interact with multiple protein targets in the histone ribonucleoprotein complex (RNP) and also facilitate its ability to be phosphorylated by different kinases.

We also show using mass spectrometry that hSLBP is phosphorylated at 23 Ser/Thr residues when expressed in a eukaryotic expression system such as baculovirus. Several sites in the hSLBP N-terminal domain and the 11 sites in the region C-terminal to the RNA binding and processing domain have also been identified in mammalian cell lines[45,56] (http://www.phosida.de/). Hyperphosphorylation and aggregation are hallmarks of many IDPs.[57] It has been shown that IDPs are on average targeted by twice as many kinases compared to folded proteins in yeast.[54] Multisite phosphorylation can help fine-tune the binding affinity and kinetics of an interaction with a binding partner depending on different conditions.[58,59] It may also regulate their cellular localization during specific phases of the cell cycle. Phosphorylation at Ser20, Ser23, Thr60, and Thr61 has been linked to SLBP degradation,[45,60] whereas phosphorylation at T171 is linked to SLBP localization and its stability.[45] Additional phosphorylation sites may regulate association of SLBP with other factors involved in histone mRNA metabolism.

Oligomerization Coupled to Phosphorylation May Regulate the Availability of SLBP to the Histone mRNP. We have shown that hSLBP can exist in two distinct complexes with hSLIP1 where the binding affinity is modulated by hSLBP phosphorylation. Whereas unphosphorylated hSLBP forms a very stable complex (K_D < 0.9 nM) with the hSLIP1 dimer, phosphorylated hSLBP forms a complex with hSLIP1 that is at least 3 orders of magnitude weaker in affinity but that can assemble on histone mRNA. We propose here that both complexes may be functionally relevant. The low-affinity complex may be required during translation, allowing hSLBP to orchestrate its interactions with multiple targets in the translation initiation complex more effectively. What is the possible biological role of the high-affinity unphosphorylated hSLBP−hSLIP1 heterotetramer that does not bind histone mRNA? We have shown that the high-affinity unphosphorylated hSLBP−hSLIP1 heterotetramer complex involves additional sequence determinants in the hSLBP RBD. We suggest that one role of hSLIP1 may be to sequester the newly synthesized hSLBP in the cytoplasm and prevent its proteolytic degradation. IDPs are particularly susceptible to ubiquitin-dependent[61] and ubiquitin-independent degradation pathways,[62] and several IDP clients are associated with "nanny"-like proteins that help protect the IDP from degradation.[63] Examples of this include Hdmx that binds the disordered transcription activation domains of p53 and p73[64] and c-Jun and c-Fos that function as part of the AP-1 complex, among many others.[63] Consistent with this hypothesis, full-length hSLBP cannot be expressed in bacteria and is prone to proteolytic degradation. Surprisingly, no proteolytic degradation of hSLBP was observed either by Western blotting or by mass spectrometry in our co-expression system with hSLIP1. Therefore, hSLIP1 may act as a guardian, protecting the newly synthesized hSLBP from degradation in vivo. Similarly, at the end of the S phase, the formation of the unphosphosphorylated hSLBP−hSLIP1 complex may facilitate removal of hSLBP from the histone mRNA, when hSLBP and histone mRNA need to be degraded.

The phosphorylation site that may be particularly relevant to regulate oligomerization of the complex lies in the hSLBP RBD at Thr171. Thr171 phosphorylation promotes formation of a monomeric hSLBP−RNA complex and may couple RNA binding activity to the oligomeric state of the complex. We show by mass spectrometry that threonine phosphorylation in the RBD in the highly conserved ^{171}TPNK sequence[44] is important for triggering the dissociation of the dimer to the monomer. Therefore, it is likely that the two hSLBP RBDs interact in the context of the unphosphorylated heterotetramer, thereby forming a high-affinity complex and occluding the RNA binding interface. Recent structural bioinformatics studies[65] suggest that phosphorylation sites in proteins tend to be enriched at protein−protein interfaces especially for hetero-oligomers. While phosphorylation has modest effects on protein conformation and stability in a third of the cases studied, phosphorylation has a large energetic effect on destabilizing a hetero-oligomeric state. Our results for the hSLBP−hSLIP1 complex are consistent with such a proposed role for phosphorylation.

Implications for the Regulation of Histone mRNAs. There is a growing body of evidence that the hSLBP−hSLIP1 complex likely functions as a complementary unit, to regulate not only the translation of histone mRNA but also other histone gene-specific processes.[66] hSLIP1 functions both in the nucleus and in the cytoplasm,[23,67] and we observe both nuclear and cytoplasmic staining by microscopy. On the basis of our study, we propose a model (Figure 7 of the Supporting

Information) for how the hSLIP1−hSLBP complex may function to regulate histone mRNA metabolism. We suggest that hSLIP1 may associate with hSLBP as an inactive heterotetramer when hSLBP is translated, thereby protecting it from proteolytic degradation in the cell. We propose that the heterotetramer is recruited to histone locus bodies, the site of transcription of histone genes. hSLBP is activated by hSLBP phosphorylation at Thr171, and the complex assembles into the histone processing complex. In support of this, hSLIP1 (or ADO23) has been reported to be important for transcription of histone H4.[68] hSLIP1 interacts with the C-terminus of the histone H4-specific transcriptional regulator HiNF-P.[68] HiNF-P physically interacts with the histone gene coactivator p220^{NPAT} and upregulates histone H4 gene transcription at the G1−S phase transition of the cell cycle. The hSLIP1−hSLBP−histone mRNA ternary complex is likely exported to the cytoplasm where it stimulates translation of histone mRNAs. At the end of the S phase, hSLBP is dephosphorylated at Thr171 by Pin1 and PP2A,[45] resulting in dissociation of the hSLIP1−hSLBP−histone mRNA ternary complex, facilitating histone mRNA decay and hSLBP ubiquitination. We speculate that hSLIP1 may aid in removal of unphosphorylated hSLBP from the histone mRNA at this time. hSLIP1 may be involved in all steps of histone biogenesis, besides translation of the mRNA, and act as a scaffold for recruitment of factors involved in regulation of histone mRNA metabolism.

The hSLIP1 homodimer is unique in the MIF4G family of proteins. The AFM data we have reported indicate that both the monomer and the dimer could exist at physiological concentrations of hSLIP1. hSLBP appears to recognize hSLIP1 near the dimer interface. We identified a single-point mutation, R202A, in hSLIP1 that abrogated binding to hSLBP. In contrast, the hSLIP1 E200A mutant that disrupted dimer formation also increased the affinity for hSLBP. This would suggest that the active complex that assembles on the histone mRNA may consist of one molecule of hSLBP and one molecule of hSLIP1 monomer. Overexpression of R202A hSLIP1 resulted in slower cell cycle progression of HeLa cells into the S phase and greater accumulation of cells in the G1 phase of the cell cycle. The R202A hSLIP1 protein also repressed histone mRNA abundance. The exact mechanism of this decreased level of expression of histone mRNA in R202A hSLIP1-expressing cells is not clear. It could result from an abrogation of the hSLBP−hSLIP1 interaction in vivo, resulting in defective histone gene transcription, processing, export, and degradation of the histone message. A detailed biological characterization of the R202A SLIP1 mutant in vivo should provide new information about the roles of hSLIP1 in regulating multiple pathways that control histone gene expression.

■ ASSOCIATED CONTENT

Supporting Information

Methods, figures, and tables. This material is available free of charge via the Internet at http://pubs.acs.org.

■ AUTHOR INFORMATION

Corresponding Author

*Telephone: (716) 898-8687. Fax: (716) 898-8660. E-mail: rthapar@hwi.buffalo.edu.

Present Address

#Department of Biochemistry and Cell Biology, Rice University, Houston, TX 77005. E-mail: rthapar@rice.edu.

Funding

These studies were supported by National Institutes of Health (NIH) Grants 1RO1-GM076660 and 1RO1-GM076660-04S1 (ARRA) to William F. Marzluff and R.T. and faculty startup funds from the Hauptman-Woodward Medical Research Institute to R.T. R.B. was supported by NIH Grant 1RO1-GM072131. Y.L.L. and L.S.S. were supported by NIH Grants 1R01-GM096039 and 1P01-GM091743.

Notes

The authors declare no competing financial interest.

■ ACKNOWLEDGMENTS

We acknowledge the Nanoimaging Core Facility at the University of Nebraska Medical Center (UNMC) for the acquisition of the AFM data. The facility was supported by grants from the National Institutes of Health [1S10 RR023400-01 (SIG program)], the UNMC Program of Excellence (POE), and the Nebraska Research Initiative (NRI). We also appreciate Mary LoPresti, Edward Z. Voss, and Jean Kanyo (W. M. Keck Foundation Biotechnology Resource Laboratory, Yale University) for assistance with preparing samples, collecting the intact mass data, and gathering the LC−MS/MS data for phosphorylation site determination, respectively. We thank Andria Denmon for critical reading of the manuscript.

■ ABBREVIATIONS

SLBP, stem−loop binding protein; SLIP1, SLBP interacting protein 1; SPR, surface plasmon resonance; NMR, nuclear magnetic resonance; AUC, analytical ultracentrifugation; MS, mass spectrometry; AFM, atomic force microscopy; CD, circular dichroism; MIF4GD, middle domain of the eukaryotic initiation factor 4G domain; UTR, untranslated region; WT, wild type; IDP, intrinsically disordered protein.

■ REFERENCES

(1) Marzluff, W. F., Wagner, E. J., and Duronio, R. J. (2008) Metabolism and regulation of canonical histone mRNAs: Life without a poly(A) tail. *Nat. Rev. Genet. 9*, 843−854.

(2) Wang, Z. F., Whitfield, M. L., Ingledue, T. C., III, Dominski, Z., and Marzluff, W. F. (1996) The protein that binds the 3′ end of histone mRNA: A novel RNA-binding protein required for histone pre-mRNA processing. *Genes Dev. 10*, 3028−3040.

(3) Dominski, Z., Sumerel, J., Hanson, R. J., and Marzluff, W. F. (1995) The polyribosomal protein bound to the 3′ end of histone mRNA can function in histone pre-mRNA processing. *RNA 1*, 915−923.

(4) Sullivan, K. D., Mullen, T. E., Marzluff, W. F., and Wagner, E. J. (2009) Knockdown of SLBP results in nuclear retention of histone mRNA. *RNA 15*, 459−472.

(5) Sanchez, R., and Marzluff, W. F. (2002) The stem-loop binding protein is required for efficient translation of histone mRNA in vivo and in vitro. *Mol. Cell. Biol. 22*, 7093−7104.

(6) Pandey, N. B., and Marzluff, W. F. (1987) The stem-loop structure at the 3′ end of histone mRNA is necessary and sufficient for regulation of histone mRNA stability. *Mol. Cell. Biol. 7*, 4557−4559.

(7) Graves, R. A., Pandey, N. B., Chodchoy, N., and Marzluff, W. F. (1987) Translation is required for regulation of histone mRNA degradation. *Cell 48*, 615−626.

(8) Whitfield, M. L., Kaygun, H., Erkmann, J. A., Townley-Tilson, W. H., Dominski, Z., and Marzluff, W. F. (2004) SLBP is associated with

histone mRNA on polyribosomes as a component of the histone mRNP. *Nucleic Acids Res. 32*, 4833−4842.
(9) Gallie, D. R., Lewis, N. J., and Marzluff, W. F. (1996) The histone 3′-terminal stem-loop is necessary for translation in Chinese hamster ovary cells. *Nucleic Acids Res. 24*, 1954−1962.
(10) Ling, J., Morley, S. J., Pain, V. M., Marzluff, W. F., and Gallie, D. R. (2002) The histone 3′-terminal stem-loop-binding protein enhances translation through a functional and physical interaction with eukaryotic initiation factor 4G (eIF4G) and eIF3. *Mol. Cell. Biol. 22*, 7853−7867.
(11) Gorgoni, B., Andrews, S., Schaller, A., Schumperli, D., Gray, N. K., and Muller, B. (2005) The stem-loop binding protein stimulates histone translation at an early step in the initiation pathway. *RNA 11*, 1030−1042.
(12) Cakmakci, N. G., Lerner, R. S., Wagner, E. J., Zheng, L., and Marzluff, W. F. (2008) SLIP1, a factor required for activation of histone mRNA translation by the stem-loop binding protein. *Mol. Cell. Biol. 28*, 1182−1194.
(13) Marintchev, A., and Wagner, G. (2005) eIF4G and CBP80 share a common origin and similar domain organization: Implications for the structure and function of eIF4G. *Biochemistry 44*, 12265−12272.
(14) Ponting, C. P. (2000) Novel eIF4G domain homologues linking mRNA translation with nonsense-mediated mRNA decay. *Trends Biochem. Sci. 25*, 423−426.
(15) Bateman, A., Birney, E., Durbin, R., Eddy, S. R., Howe, K. L., and Sonnhammer, E. L. (2000) The Pfam protein families database. *Nucleic Acids Res. 28*, 263−266.
(16) Marcotrigiano, J., Lomakin, I. B., Sonenberg, N., Pestova, T. V., Hellen, C. U., and Burley, S. K. (2001) A conserved HEAT domain within eIF4G directs assembly of the translation initiation machinery. *Mol. Cell 7*, 193−203.
(17) Craig, A. W., Haghighat, A., Yu, A. T., and Sonenberg, N. (1998) Interaction of polyadenylate-binding protein with the eIF4G homologue PAIP enhances translation. *Nature 392*, 520−523.
(18) Levy-Strumpf, N., Deiss, L. P., Berissi, H., and Kimchi, A. (1997) DAP-5, a novel homolog of eukaryotic translation initiation factor 4G isolated as a putative modulator of γ interferon-induced programmed cell death. *Mol. Cell. Biol. 17*, 1615−1625.
(19) LaRonde-LeBlanc, N., Santhanam, A. N., Baker, A. R., Wlodawer, A., and Colburn, N. H. (2007) Structural basis for inhibition of translation by the tumor suppressor Pdcd4. *Mol. Cell. Biol. 27*, 147−156.
(20) Kadlec, J., Izaurralde, E., and Cusack, S. (2004) The structural basis for the interaction between nonsense-mediated mRNA decay factors UPF2 and UPF3. *Nat. Struct. Mol. Biol. 11*, 330−337.
(21) Kim, K. M., Cho, H., Choi, K., Kim, J., Kim, B. W., Ko, Y. G., Jang, S. K., and Kim, Y. K. (2009) A new MIF4G domain-containing protein, CTIF, directs nuclear cap-binding protein CBP80/20-dependent translation. *Genes Dev. 23*, 2033−2045.
(22) Mazza, C., Ohno, M., Segref, A., Mattaj, I. W., and Cusack, S. (2001) Crystal structure of the human nuclear cap binding complex. *Mol. Cell 8*, 383−396.
(23) Neusiedler, J., Mocquet, V., Limousin, T., Ohlmann, T., Morris, C., and Jalinot, P. (2012) INT6 interacts with MIF4GD/SLIP1 and is necessary for efficient histone mRNA translation. *RNA 18*, 1163−1177.
(24) Bae, E., Bitto, E., Bingman, C. A., McCoy, J. G., Wesenberg, G. E., and Phillips, G. N., Jr. (2010) Crystal structure of an eIF4G-like protein from *Danio rerio*. *Proteins 78*, 1803−1806.
(25) Andrade, M. A., and Bork, P. (1995) HEAT repeats in the Huntington's disease protein. *Nat. Genet. 11*, 115−116.
(26) Dominski, Z., Yang, X. C., Raska, C. S., Santiago, C., Borchers, C. H., Duronio, R. J., and Marzluff, W. F. (2002) 3′ end processing of *Drosophila melanogaster* histone pre-mRNAs: Requirement for phosphorylated *Drosophila* stem-loop binding protein and coevolution of the histone pre-mRNA processing system. *Mol. Cell. Biol. 22*, 6648−6660.
(27) Farrow, N. A., Zhang, O., Forman-Kay, J. D., and Kay, L. E. (1997) Characterization of the backbone dynamics of folded and denatured states of an SH3 domain. *Biochemistry 36*, 2390−2402.
(28) Stafford, W. F., III (1994) Boundary analysis in sedimentation velocity experiments. *Methods Enzymol. 240*, 478−501.
(29) Liu, S., and Stafford, W. F., III (1995) An optical thermometer for direct measurement of cell temperature in the Beckman instruments XL-A analytical ultracentrifuge. *Anal. Biochem. 224*, 199−202.
(30) Stafford, W. F., and Sherwood, P. J. (2004) Analysis of heterologous interacting systems by sedimentation velocity: Curve fitting algorithms for estimation of sedimentation coefficients, equilibrium and kinetic constants. *Biophys. Chem. 108*, 231−243.
(31) Laue, T. M., Shah, B. D., Ridgeway, T. M., and Pelletier, S. L. (1992) Computer aided interpretation of analytical sedimentation data for proteins. *Analytical Ultracentrifugation in Biochemistry and Polymer Sciences* (Harding, R. A., and Horton, J. C., Eds.) Royal Society of Chemistry, Cambridge, U.K.
(32) Shlyakhtenko, L. S., Gall, A. A., Filonov, A., Cerovac, Z., Lushnikov, A., and Lyubchenko, Y. L. (2003) Silatrane-based surface chemistry for immobilization of DNA, protein-DNA complexes and other biological materials. *Ultramicroscopy 97*, 279−287.
(33) Lyubchenko, Y. L., Shlyakhtenko, L. S., and Gall, A. A. (2009) Atomic force microscopy imaging and probing of DNA, proteins, and protein DNA complexes: Silatrane surface chemistry. *Methods Mol. Biol. 543*, 337−351.
(34) Lyubchenko, Y. L., and Shlyakhtenko, L. S. (2009) AFM for analysis of structure and dynamics of DNA and protein-DNA complexes. *Methods 47*, 206−213.
(35) Shlyakhtenko, L. S., Lushnikov, A. Y., Miyagi, A., Li, M., Harris, R. S., and Lyubchenko, Y. L. (2012) Nanoscale structure and dynamics of ABOBEC3G complexes with single-stranded DNA. *Biochemistry 51*, 6432−6440.
(36) Ashkenazy, H., Erez, E., Martz, E., Pupko, T., and Ben-Tal, N. (2010) ConSurf 2010: Calculating evolutionary conservation in sequence and structure of proteins and nucleic acids. *Nucleic Acids Res. 38*, W529−W533.
(37) Zheng, L., Dominski, Z., Yang, X. C., Elms, P., Raska, C. S., Borchers, C. H., and Marzluff, W. F. (2003) Phosphorylation of stem-loop binding protein (SLBP) on two threonines triggers degradation of SLBP, the sole cell cycle-regulated factor required for regulation of histone mRNA processing, at the end of S phase. *Mol. Cell. Biol. 23*, 1590−1601.
(38) Dyson, H. J., and Wright, P. E. (2004) Unfolded proteins and protein folding studied by NMR. *Chem. Rev. 104*, 3607−3622.
(39) Junius, F. K., Mackay, J. P., Bubb, W. A., Jensen, S. A., Weiss, A. S., and King, G. F. (1995) Nuclear magnetic resonance characterization of the Jun leucine zipper domain: Unusual properties of coiled-coil interfacial polar residues. *Biochemistry 34*, 6164−6174.
(40) Croasdale, R., Ivins, F. J., Muskett, F., Daviter, T., Scott, D. J., Hardy, T., Smerdon, S. J., Fry, A. M., and Pfuhl, M. (2011) An undecided coiled coil: The leucine zipper of Nek2 kinase exhibits atypical conformational exchange dynamics. *J. Biol. Chem. 286*, 27537−27547.
(41) Thapar, R., Mueller, G. A., and Marzluff, W. F. (2004) The N-terminal domain of the *Drosophila* histone mRNA binding protein, SLBP, is intrinsically disordered with nascent helical structure. *Biochemistry 43*, 9390−9400.
(42) Pellecchia, M., Montgomery, D. L., Stevens, S. Y., Vander Kooi, C. W., Feng, H. P., Gierasch, L. M., and Zuiderweg, E. R. (2000) Structural insights into substrate binding by the molecular chaperone DnaK. *Nat. Struct. Biol. 7*, 298−303.
(43) Hall, D. A., Vander Kooi, C. W., Stasik, C. N., Stevens, S. Y., Zuiderweg, E. R., and Matthews, R. G. (2001) Mapping the interactions between flavodoxin and its physiological partners flavodoxin reductase and cobalamin-dependent methionine synthase. *Proc. Natl. Acad. Sci. U.S.A. 98*, 9521−9526.
(44) Borchers, C. H., Thapar, R., Petrotchenko, E. V., Torres, M. P., Speir, J. P., Easterling, M., Dominski, Z., and Marzluff, W. F. (2006)

Combined top-down and bottom-up proteomics identifies a phosphorylation site in stem-loop-binding proteins that contributes to high-affinity RNA binding. *Proc. Natl. Acad. Sci. U.S.A. 103*, 3094−3099.
(45) Krishnan, N., Lam, T. T., Fritz, A., Rempinski, D., O'Loughlin, K., Minderman, H., Berezney, R., Marzluff, W. F., and Thapar, R. (2012) The Prolyl Isomerase Pin1 Targets Stem-Loop Binding Protein (SLBP) To Dissociate the SLBP-Histone mRNA Complex Linking Histone mRNA Decay with SLBP Ubiquitination. *Mol. Cell. Biol. 32*, 4306−4322.
(46) Miyagi, A., Tsunaka, Y., Uchihashi, T., Mayanagi, K., Hirose, S., Morikawa, K., and Ando, T. (2008) Visualization of intrinsically disordered regions of proteins by high-speed atomic force microscopy. *ChemPhysChem 9*, 1859−1866.
(47) Turoverov, K. K., Kuznetsova, I. M., and Uversky, V. N. (2010) The protein kingdom extended: Ordered and intrinsically disordered proteins, their folding, supramolecular complex formation, and aggregation. *Prog. Biophys. Mol. Biol. 102*, 73−84.
(48) Uversky, V. N. (2009) Intrinsic disorder in proteins associated with neurodegenerative diseases. *Front. Biosci. 14*, 5188−5238.
(49) Zhang, M., Lam, T. T., Tonelli, M., Marzluff, W. F., and Thapar, R. (2012) Interaction of Histone mRNA Hairpin with Stem-Loop Binding Protein and Regulation of the SLBP-RNA Complex by Phosphorylation and Proline Isomerization. *Biochemistry 51*, 3215−3231.
(50) Dimitrova, D. S., and Berezney, R. (2002) The spatio-temporal organization of DNA replication sites is identical in primary, immortalized and transformed mammalian cells. *J. Cell Sci. 115*, 4037−4051.
(51) Nakayasu, H., and Berezney, R. (1989) Mapping replicational sites in the eucaryotic cell nucleus. *J. Cell Biol. 108*, 1−11.
(52) Wright, P. E., and Dyson, H. J. (1999) Intrinsically unstructured proteins: Re-assessing the protein structure-function paradigm. *J. Mol. Biol. 293*, 321−331.
(53) Ward, J. J., Sodhi, J. S., McGuffin, L. J., Buxton, B. F., and Jones, D. T. (2004) Prediction and functional analysis of native disorder in proteins from the three kingdoms of life. *J. Mol. Biol. 337*, 635−645.
(54) Gsponer, J., Futschik, M. E., Teichmann, S. A., and Babu, M. M. (2008) Tight regulation of unstructured proteins: From transcript synthesis to protein degradation. *Science 322*, 1365−1368.
(55) Iakoucheva, L. M., Radivojac, P., Brown, C. J., O'Connor, T. R., Sikes, J. G., Obradovic, Z., and Dunker, A. K. (2004) The importance of intrinsic disorder for protein phosphorylation. *Nucleic Acids Res. 32*, 1037−1049.
(56) Gnad, F., Gunawardena, J., and Mann, M. (2011) PHOSIDA 2011: The posttranslational modification database. *Nucleic Acids Res. 39*, D253−D260.
(57) Chiti, F., and Dobson, C. M. (2006) Protein misfolding, functional amyloid, and human disease. *Annu. Rev. Biochem. 75*, 333−366.
(58) Honnappa, S., Jahnke, W., Seelig, J., and Steinmetz, M. O. (2006) Control of intrinsically disordered stathmin by multisite phosphorylation. *J. Biol. Chem. 281*, 16078−16083.
(59) Braithwaite, S. P., Stock, J. B., and Mouradian, M. M. (2012) α-Synuclein phosphorylation as a therapeutic target in Parkinson's disease. *Rev. Neurosci. 23*, 191−198.
(60) Koseoglu, M. M., Graves, L. M., and Marzluff, W. F. (2008) Phosphorylation of threonine 61 by cyclin a/Cdk1 triggers degradation of stem-loop binding protein at the end of S phase. *Mol. Cell. Biol. 28*, 4469−4479.
(61) Hershko, A., and Ciechanover, A. (1998) The ubiquitin system. *Annu. Rev. Biochem. 67*, 425−479.
(62) Tsvetkov, P., Reuven, N., and Shaul, Y. (2010) Ubiquitin-independent p53 proteasomal degradation. *Cell Death Differ. 17*, 103−108.
(63) Tsvetkov, P., Reuven, N., and Shaul, Y. (2009) The nanny model for IDPs. *Nat. Chem. Biol. 5*, 778−781.
(64) Tsvetkov, P., Reuven, N., Prives, C., and Shaul, Y. (2009) Susceptibility of p53 unstructured N terminus to 20 S proteasomal degradation programs the stress response. *J. Biol. Chem. 284*, 26234−26242.
(65) Nishi, H., Hashimoto, K., and Panchenko, A. R. (2011) Phosphorylation in protein-protein binding: Effect on stability and function. *Structure 19*, 1807−1815.
(66) Mitra, P., Xie, R. L., Medina, R., Hovhannisyan, H., Zaidi, S. K., Wei, Y., Harper, J. W., Stein, J. L., van Wijnen, A. J., and Stein, G. S. (2003) Identification of HiNF-P, a key activator of cell cycle-controlled histone H4 genes at the onset of S phase. *Mol. Cell. Biol. 23*, 8110−8123.
(67) Smith, T. C., Fang, Z., and Luna, E. J. (2010) Novel interactors and a role for supervillin in early cytokinesis. *Cytoskeleton 67*, 346−364.
(68) Miele, A., Medina, R., van Wijnen, A. J., Stein, G. S., and Stein, J. L. (2007) The interactome of the histone gene regulatory factor HiNF-P suggests novel cell cycle related roles in transcriptional control and RNA processing. *J Cell. Biochem. 102*, 136−148.